Elsevier Editorial System(tm) for Journal of Human Evolution

Manuscript Draft

Manuscript Number: HUMEV-P-15-00039R3

Title: The morphology of the enamel-dentine junction in Neanderthal molars: gross morphology, non-metric traits, and temporal trends

Article Type: Full Length Article

Keywords: Neanderthal; EDJ; molars; microCT; dental morphology; discrete dental traits

Corresponding Author: Dr. Matthew Skinner, Ph.D.

Corresponding Author's Institution: University of Kent

First Author: Robert G Martin

Order of Authors: Robert G Martin; Jean-Jacques Hublin; Philipp Gunz; Matthew Skinner, Ph.D.

Abstract: This study explores the morphological differences between the enamel-dentine junction (EDJ) of maxillary and mandibular molars of Neanderthals (n = 150) and recent modern humans (n = 106), and between an earlier Neanderthal sample (consisting of Pre-Eemian and Eemian Neanderthals dating to before 115 ka) and a later Neanderthal sample (consisting of Post-Eemian Neanderthals dating to after 115 ka). The EDJ was visualised by segmenting microtomographic scans of each molar. A geometric morphometric methodology compared the positioning of the dentine horns, the shape of the marginal ridge between the dentine horns, and the shape of the cervix. We also examined the manifestation of non-metric traits at the EDJ including the crista obliqua, cusp 5, and post-paracone tubercle. Furthermore, we report on additional morphological features including centrally placed dentine horn tips and twinned dentine horns. Our results indicate that EDJ morphology can discriminate with a high degree of reliability between Neanderthals and recent modern humans at every molar position, and discriminate between the earlier and the later Neanderthal samples at every molar position, except for the M3 in shape space. The cervix in isolation can also discriminate between Neanderthals and recent modern humans, except at the M3 in form space and is effective at discriminating between the earlier and the later Neanderthal samples, except at the M2/M2 in form space. In addition to demonstrating the taxonomic valence of the EDJ, our analysis reveals unique manifestations of dental traits in Neanderthals and expanded levels of trait variation that have implications for trait definitions and scoring.

Detailed Response to Reviewers

Dear Mike,

I just put this in as the revision required a ‘response to review’. I have uploaded the new revision with the copy-edits.

Kind regards, Matt

The morphology of the enamel-dentine junction in Neanderthal molars: gross morphology, non-metric traits, and temporal trends

Robert M. G. Martin[1], Jean-Jacques Hublin[2], Philipp Gunz[2], Matthew M. Skinner*[2, 3]

[1]Department of Anthropology, University of Toronto, 19 Russell Street, Toronto M5S 2S2, Canada
[2]Department of Human Evolution, Max Planck Institute for Evolutionary Anthropology, Deutscher Platz 6, 04103 Leipzig, Germany
[3]School of Anthropology and Conservation, University of Kent, Canterbury CT2 7NZ, United Kingdom

*Corresponding author

~~Keywords: Neanderthal; EDJ; molars; microCT; dental morphology; non-metric dental traits~~

Correspondence to: Matthew M. Skinner, School of Anthropology and Conservation, University of Kent, Canterbury, UK. Email: m.skinner@kent.ac.uk

ABSTRACT

This study explores the morphological differences between the enamel-dentine junction (EDJ) of maxillary and mandibular molars of Neanderthals (*n* = 150) and recent modern humans (*n* = 106), and between an earlier Neanderthal sample (consisting of Pre-Eemian and Eemian Neanderthals dating to before 115 ka) and a later Neanderthal sample (consisting of Post-Eemian Neanderthals dating to after 115 ka). The EDJ was visualised by segmenting microtomographic scans of each molar. A geometric morphometric methodology compared the positioning of the dentine horns, the shape of the marginal ridge between the dentine horns, and the shape of the cervix. We also examined the manifestation of non-metric traits at the EDJ including the crista obliqua, cusp 5, and post-paracone tubercle. Furthermore, we report on additional morphological features including centrally placed dentine horn tips and twinned dentine horns. Our results indicate that EDJ morphology can discriminate with a high degree of reliability between Neanderthals and recent modern humans at every molar position, and discriminate between the earlier and the later Neanderthal samples at every molar position, except for the M_3 in shape space. The cervix in isolation can also discriminate between Neanderthals and recent modern humans, except at the M_3 in form space and is effective at discriminating between the earlier and the later Neanderthal samples, except at the M^2/M_2 in form space. In addition to demonstrating the taxonomic valence of the EDJ, our analysis reveals unique manifestations of dental traits in Neanderthals and expanded levels of trait variation that have implications for trait definitions and scoring.

Keywords: Neanderthal; EDJ; molars; microCT; dental morphology; non-metric dental traits

Introduction

Teeth carry a strong taxonomic and phylogenetic signal and serve an important role in making systematic inferences about fossil hominins (e.g., Weidenreich, 1937; Robinson, 1956; Trinkhaus, 1978; Johanson and White, 1979; Wolpoff, 1979; Wood and Abbott, 1983; Suwa et al., 1994; Bermúdez de Castro et al., 1999; Bailey, 2006; Martinón-Torres et al., 2012). This is due to the predominance of teeth in the hominin fossil record, the fact that teeth do not remodel (except through attrition or decay), and because tooth development responsible for cusp formation and positioning is tightly controlled by genetics (Jernvall and Jung, 2000; Thesleff, 2000, 2006). The dentition of *Homo neanderthalensis* (hereafter Neanderthals) and recent *Homo sapiens* (hereafter referred to as recent modern humans) has been studied extensively and has been central to hypotheses regarding the position of Neanderthals relative to other Middle Pleistocene hominins and differentiating them as a distinct species from recent modern humans (Tyrrell and Chamberlain, 1998; Bermúdez de Castro et al., 1999; Bailey, 2002, 2004; Harvati et al., 2003; Bailey and Hublin, 2006; Macchiarelli et al., 2006; Martinón-Torres et al., 2006, 2013; Benazzi et al., 2012; Gómez-Robles et al., 2012; Zanolli and Mazurier, 2013; Bailey et al., 2014). In this contribution, we expand on these previous studies by providing novel data on the internal structure of a large sample of Neanderthal and recent modern human maxillary and mandibular molars.

Previous studies of Neanderthal dental morphology have focused on a number of aspects of the outer enamel surface (OES), including analyses of non-metric traits and overall crown and cusp morphology (Wolpoff, 1979; Wolpoff et al., 1981; Smith et al., 1982; Bailey, 2002, 2004, 2006; Bailey and Lynch, 2005; Martinón-Torres et al., 2006, 2013; Gómez-Robles et al., 2007, 2008, 2012; Benazzi et al., 2011a, 2011b, 2012). For the most part, these studies have indicated that Neanderthals have a distinct and derived dental morphology, including a unique pattern of non-metric dental trait frequencies in comparison to contemporary and fossil modern humans. For example, two-dimensional geometric morphometric studies have found the M^1 (Bailey, 2004; Gómez-Robles et al., 2007; Benazzi et al., 2011a) and the M_1 (Benazzi et al., 2011a) of Neanderthals to be morphologically

distinct from recent modern humans. However, 2D geometric morphometric studies have also found that the shape of the OES does not effectively discriminate the M^2 and M^3 of Neanderthals when classified against recent modern humans and Middle Pleistocene European hominins (Gómez-Robles et al., 2012). Distinctive patterns of dental trait expression at the OES have been demonstrated for a number of tooth positions (Bailey, 2002, 2006).

A number of studies have noted temporal variation in the distribution and frequency of derived versus primitive skeletal features among the Late Middle and Upper Pleistocene western Eurasian hominins (e.g., Howell, 1960; Arsuaga et al., 1997; Hublin 1998) leading to the formulation of various evolutionary models (e.g., Rosas et al., 2006; Hublin, 2009; Dennell et al., 2011; Bermúdez de Castro and Martinón-Torres, 2013). In particular these models diverge on the level of continuity and gradualism observed among these populations. While Rosas et al. (2006) support the succession of two morphologically stable paleospecies (*H. heidelbergensis* and *H. neanderthalensis*), Hublin (2009) supports a gradual change among the European populations with an increase in frequency of the derived Neanderthal conditions already starting in the middle of the Middle Pleistocene (so-called "accretion model"). Bermúdez de Castro and Martinón-Torres (2013) argue for a succession of demes coming from an external geographical source and occasionally interbreeding. Recent genetic analyses indicate that the Sima de los Huesos fossils are already part of the Neanderthal lineage (Meyer et al., 2016). This result, together with the recent morphological reassessment of the Sima de los Huesos material (Arsuaga et al., 2014), supports the accretion model and provides a first appearance date for some Neanderthal specific morphology at approximately 430 ka. With the archaeological evidence from Gorham's Cave, Gibraltar indicating a last appearance date of 28 ka (Finlayson et al., 2006; but see also Wood et al., 2013) the Neanderthal lineage spans approximately 400 ky. Although we do not have access to the material from Sima de los Huesos, material from earlier Neanderthal sites such as Krapina, Abri Suard, and Abri Bourgeois-Delaunay allows us to examine whether there are temporal trends in maxillary and mandibular molar shape, which would support particular models of Neanderthal evolution. Furthermore, given recent genetic studies that

indicate that Neanderthals and recent modern humans interbred, raising the possibility for a genetic contribution from Neanderthals to recent modern human dental morphology (Green et al., 2010; Meyer et al., 2012, Prüfer et al., 2014; Fu et al., 2015), it is particularly timely to characterise in detail the morphology of Neanderthal molars relative to those of recent modern humans.

New imaging techniques have made it possible to study the internal structures of teeth in high resolution and extract novel morphological data that can be brought to bear on taxonomic and phylogenetic questions. One such structure, the enamel-dentine junction (EDJ), is the interface between the enamel cap and the coronal dentine (Butler, 1956, 1999). The EDJ approximates the inner enamel epithelium of the developing tooth germ and has been shown in previous analyses to provide unique information about the developmental processes underlying tooth crown growth (Kraus, 1952; Korenhof, 1961, 1982; Kraus and Jordan, 1965; Skinner and Gunz, 2010; Skinner et al., 2010), and taxonomic and phylogenetic information (Corruccini, 1987, 1998; Macchiarelli et al., 2006; Skinner et al., 2008a, 2008b, 2009a, 2010; Bailey et al., 2011). EDJ morphology has also been used to successfully discriminate closely related species of extant ape and fossil hominins, as well as differentiate between molar positions along the tooth row (Skinner et al., 2008a, 2008b, 2009a; Braga et al., 2010; Zanolli et al., 2012, 2014, 2015; Zanolli and Mazurier, 2013; Zanolli, 2015). Recently, a number of studies have examined the EDJ of Neanderthal teeth, focusing on non-metric trait expression (Macchiarelli et al., 2006; Skinner et al., 2008c; Bailey et al., 2011; Martínez de Pinillos et al., 2014; Martinón-Torres et al., 2014).

Non-metric traits are particularly useful for determining phylogenetic relationships (Robinson, 1956; Wood and Abbot, 1983; Aiello and Dean, 2002; Bailey 2002, 2006; Guatelli-Steinberg and Irish, 2005; Irish et al., 2013) and most studies of non-metric traits in Neanderthal molars have focused on the OES and have used human standards (e.g., ASUDAS, or the Arizona State University Dental Anthropology System) (Turner et al., 1991). Difficulties in applying human standards to the study of Neanderthal teeth have been noted in past studies because many traits that are rare or absent in recent modern humans, but present in Neanderthals, are excluded from

the standard scoring procedure in ASUDAS (Bailey, 2002, 2006). This problem is two-fold when studying the EDJ of Neanderthals, because ASUDAS was developed for the OES, and a standardised scoring system for non-metric traits at the EDJ has yet to be developed (Skinner et al., 2008c, 2009b; Ortiz et al., 2012). We hypothesise, based on the results of studies cited above, that examining the EDJ manifestation of non-metric traits in a large sample of Neanderthals will reveal previously unappreciated variation in trait morphology, elucidate trait development and provide critical evidence for the future application of trait scoring systems in the hominin clade.

The patterning cascade model (PCM) of development predicts that tooth development is an iterative process, where successive cusps form along the tooth using the same developmental pathway, and that while cusps form, there is a zone of inhibition that prevents more cusps from forming in close proximity, and any simultaneous cusp development would need to be initiated outside that zone of inhibition (Polly, 1998; Jernvall, 2000; Jernvall and Jung, 2000; Jernvall and Thesleff, 2000; Salazar-Ciudad and Jernvall, 2002, 2010; Kangas et al., 2004; Kassai et al., 2005). This means that the size and shape of the primary cusps will influence the formation of any secondary cusps. Observations of the EDJ in the mandibular molars of chimpanzees are consistent with the PCM of development (Skinner and Gunz, 2010). Thus, a focus of this study is to interpret variation in crown morphology and, in particular, the definition, presence, and degree of expression of non-metric traits at the EDJ with reference to the predictions of the PCM.

Using microtomography and 3D geometric morphometrics of the EDJ surface, this study addresses the following questions: 1) how distinct is mandibular and maxillary molar morphology between Neanderthals and recent modern humans, and between earlier and later Neanderthal samples; 2) does the frequency and/or expression of non-metric traits at the EDJ differ between Neanderthals and recent modern humans, and between earlier and later Neanderthal samples; and 3) is the PCM of development consistent with the expression of non-metric traits at the Neanderthal EDJ?

Materials

The study sample is shown in Table 1. The sample consists of 256 maxillary and mandibular molars attributed to Neanderthals (*n* = 150) and recent modern humans (*n* = 106). The Neanderthal specimens were subdivided by published geochronological age into two samples: an earlier Neanderthal sample (consisting of Pre-Eemian and Eemian Neanderthals dating to before 115 ka) and a later Neanderthal sample (consisting of Post-Eemian Neanderthals dating to after 115 ka) (Dahl-Jensen et al., 2013). Approximately 79% of the earlier Neanderthal sample is derived from Krapina, Croatia, and approximately 25% of the later Neanderthal sample is derived from El Sidrón, Spain. The earlier Neanderthal sample covers a period from about 230 to 115 ka, and the later Neanderthal sample covers a period from about 115 to 40 ka. Sex is unknown for most of the fossil specimens, so the comparative sample of recent modern humans was not divided by sex. Molar position is critically important to this study and our basis for the inferred position of each molar is listed in the Supplementary Online Material (SOM) Table S1. For example, molars can derive directly from either a mandible or maxilla (basis = 1), molar position can be inferred from an associated dentition (basis = 2), or molar position can be inferred based on previous morphological analyses by other researchers (basis = 3). Finally, the EDJ of all molars were subject to an initial geometric morphometric analysis of shape (see below) to evaluate their positions and double-check molars whose position was inferred by previous researchers based only on morphology (i.e., basis 3). From this initial analysis, the positions of seven molars were reassigned and given a basis of 4. Of these seven, all but one specimen derive from Krapina, and while not stated explicitly, as far we can determine from the relevant publications (Wolpoff, 1979; Radovčić et al., 1988), the molar position for these specimens was based on morphological grounds only (and thus is uncertain). The seventh molar is Combe Grenal IX (assigned by us as an M^1 rather than an as M^2 by Garralda and Vandermeersch [2000] based on morphological grounds only). Reassignment was only accepted if the molar in question classified consistently to a particular molar position (see Methods, Analysis of EDJ shape). Since this was the case for all seven molars, these were included in the study using their

reassigned molar positions. A list of these reassigned molars showing their old and new positions is shown in Table 2.

Methods

Microtomography

Microtomography was used to image the internal structures of the molars in the study sample. These scans were performed by the Department of Human Evolution, Max Planck Institute for Evolutionary Anthropology with either a BIR ACTIS 225/300 (kV, 100 µA, 0.25 brass filter) or a SkyScan 1172 (100 kV, 94 µA, 2.0 mm aluminium and copper filter) microtomographic scanner. The isometric voxel sizes resulting from these scans range between 15 and 50 micrometers (µm).

Image processing and surface model generation

The complete image stacks of each tooth were filtered using a three-dimensional median filter with a kernel size of 1 or 3 followed by a mean of least variance filter with a kernel size of 1 or 3. Filtering the image stacks improves grayscale homogeneity within a particular tissue, and facilitates the manual segmentation of a tooth into its enamel and dentine components (Wollny et al., 2013). Filtering has been previously shown to have a minimal effect on the morphology of dental structures present on the EDJ (Skinner, 2008). The filtered image stacks were imported into Avizo 6.3 (www.vsg3D.com), where the enamel and dentine were segmented semi-automatically using the 3D voxel value histogram and grayscale values. In Avizo 6.3, using the unconstrained smoothing parameter, the EDJ was reconstructed from the segmentation as a triangle-based surface model in .ply format. As a result of dental wear, the tips of the dentine horns of some specimens were missing. In such cases, dentine horn tips were reconstructed in Geomagic Studio 2012 (www.geomagic.com) relying on the preserved adjacent portions of the EDJ to estimate the original height and position of the dentine horn tip (all specimens with reconstructed dentine horns are listed in the SOM Table S2). We used our experience, anatomical knowledge, and preserved

morphology to decide when a dentine horn could be reconstructed but as a general rule it is not possible if more than ~1/3 of the dentine horn appears to be missing. Heavily worn specimens (i.e., specimens for which it was not possible to reconstruct missing dentine horns) were included in the cementum enamel junction (CEJ) analyses but excluded from the EDJ/CEJ analyses (see below).

Collection of landmarks

Three sets of 3D landmarks were collected following a previously published methodology (Skinner, 2008; Skinner et al., 2008a, 2009a; Skinner and Gunz, 2010) that is described here in brief. The first two sets of landmarks, 'EDJ_MAIN' and 'EDJ_RIDGE', were collected in Avizo 6.3 on the EDJ surface models that were generated from the segmentations. The EDJ_MAIN landmark set consists of four anatomical landmarks placed on the tips of the dentine horns of the four primary cusps of the mandibular (protoconid, metaconid, entoconid, and hypoconid) and maxillary (protocone, paracone, metacone, and hypocone) molars. In some cases the expression of the hypocone was diminutive. In these instances, the placement of the landmark was approximated based on the positions of these dentine horns on other specimens. Specimens in which cusp homology was uncertain were excluded from the sample. The only Neanderthal tooth available for study that was excluded from the EDJ analysis for this reason was El Sidrón SD406, an M_3. In this specimen the buccal marginal ridge is abnormal and it is not possible, in our opinion, to identify the distal dentine horn as a hypoconid or hypoconulid). The EDJ_RIDGE landmark set was collected by placing landmarks along the marginal ridge that connects the dentine horns. In the mandibular molars, the placement of the EDJ_RIDGE landmarks begins at the tip of the protoconid dentine horn and continues in the mesial direction. In the maxillary molars, the placement of the EDJ_RIDGE landmarks begins at the tip of the protocone dentine horn and continues in the mesial direction. Enough landmarks were placed to ensure that the variation along the marginal ridge of the EDJ was captured, and therefore this number varied between specimens. The third set of landmarks, 'CEJ_RIDGE', was collected on an isosurface rendered from the unfiltered TIFF image stacks of each

molar. In cases where a build-up of calculus prevented landmarking around the circumference of the CEJ, landmarks were placed directly on cross-sectional slices positioned appropriately within the 3D tomographic volume. For the mandibular molars, the initial CEJ landmark was placed on the mesiobuccal corner of the crown (beneath the protoconid) and continued mesially. In the maxillary molars, the initial landmark was placed on the middle part of the buccal face of the crown (between the paracone and metacone) and continued mesially. Enough landmarks were placed to ensure that the variation along the CEJ was captured. In some cases where parts of the CEJ were missing, the location was estimated. An illustration of the placement of these landmark sets is shown in Figure 1.

Derivation of homologous landmark sets

For each specimen, geometrically homologous landmarks and semilandmarks (Bookstein, 1997) were derived in Mathematica 8.0 (www.wolfram.com) using a software routine developed by Philipp Gunz (Gunz et al., 2005; Skinner et al., 2008a; Gunz and Mitteroecker, 2013). A cubic-spline function was used to fit a smooth curve through the landmarks of the EDJ_RIDGE and CEJ_RIDGE landmark sets described above. In the case of the curve generated for the EDJ_RIDGE landmark set, the EDJ_MAIN landmarks were projected onto the curve, which divided the curve into four sections. A fixed number of equally spaced landmarks were determined on each section of the curve. In the case of the mandibular molars: 12 landmarks between the protoconid and metaconid; 12 landmarks between the metaconid and entoconid; 24 landmarks between the entoconid and hypoconid; 12 landmarks between the hypoconid and protoconid; and 30 landmarks were derived along the CEJ_RIDGE spline curve. In the case of the maxillary molars: 18 landmarks between the protocone and paracone; 15 landmarks between the paracone and metacone; 15 landmarks between the metacone and hypocone; 12 landmarks between the hypocone and protocone; and 30 landmarks were placed along the CEJ_RIDGE spline curve. A generalised least squares Procrustes superimposition was performed on the landmarks to scale each landmark set to unit centroid size and to remove information about the orientation and location from the raw landmark data (Gower,

1975; Rohlf and Slice, 1990; Goodall, 1991; Dryden and Mardia, 1998). The only fixed landmarks were the EDJ_MAIN landmarks while the EDJ_RIDGE and CEJ_RIDGE landmarks were treated as semilandmarks and were permitted to slide along their curves. Sliding semilandmarks along their curves is done in such a manner that minimises the bending energy of the thin-plate spline interpolation function calculated between the Procrustes average of the sample and each specimen, and is performed to prevent visualisation artefacts resulting from equal spacing (Gunz et al., 2005; Gunz and Mitteroecker, 2013). Procrustes superimposition was applied after each sliding event and the landmarks of each specimen were considered to be geometrically correspondent after the sliding function was applied twice.

Analysis of EDJ shape

Analyses were conducted on two sets of landmarks, an EDJ/CEJ analysis, which included the curves along the marginal ridge of the EDJ and the CEJ, and a CEJ only analysis (Table 1 notes which specimens were included in each analysis). Analyses were carried out in both shape space and form space (the latter including the log of centroid size as a variable along with the Procrustes coordinates). A principal component analysis (PCA) was performed on the homologous Procrustes coordinates to examine EDJ/CEJ or CEJ shape variation in the sample (Bookstein, 1991). A canonical variate analysis (CVA) uses a linear combination of variables to maximise the ratio of between group variation to within group variation, and was used to classify molars by taxon for the purposes of assessing classification accuracy (Skinner et al., 2008a). The CVA used cross-validation to avoid over-fitting (Kovarovic et al., 2011). In a cross-validated CVA, each specimen is considered unknown before being classified against the remaining sample.

Typically in a CVA, the number of variables should be less than the number of specimens in the sample, but this is rarely possible when analysing fossil specimens, where the number of landmarks almost always exceeds the number of specimens (Hair et al., 1998~~; Strauss, 2010~~). To circumvent this problem, the CVA was performed using principal components (PCs). As there is no

clear criteria for the number of PCs to include in a CVA analysis, and the classification of individual specimens can change depending on how many PCs are used, we used sets of PCs that ranged between five and the number of PCs required to explain 95% of the variation in the PCA of each molar position for each analysis. For example, the CVA was calculated using inclusive sets of PCs 1-5, 1-6, 1-7, 1-8, 1-9, etc. A specimen was considered to have classified consistently if it classified at least 80% of the time to one taxon across each set of CVAs. The PCAs and CVAs were performed in R (www.r-project.org).

Visualisation of EDJ shape variation

Wire frames were generated in Mathematica 8.0 using a routine written by PG to show the mean landmark configuration (in this case the EDJ ridge and CEJ curves) of each tooth position of each taxon. These wire frames were superimposed to compare changes in EDJ morphology between taxa at each particular molar position and within taxa between molar positions.

Molar size

After the molars were grouped by tooth position and taxa, SPSS (www.ibm.com) was used to perform a Kruskal-Wallis one-way analysis of variance test (Kruskal and Wallis, 1952) to determine if there was a significant difference in the natural logarithm of the centroid size of molars between taxa at each molar position, and within taxa between molar positions. This analysis excluded specimens with only CEJ_RIDGE landmarks.

Non-metric traits

Preliminary observations of EDJ morphology in the Neanderthal sample revealed a number of morphological features that cannot be presented within traditional descriptions of non-metric traits based on the outer enamel surface. Below we outline these features and present the methodology used to analyse their presence and degree of expression.

Centrally placed dentine horn tips Our examination of dentine horn tips revealed variation in their position relative to the marginal ridge, with some located on the marginal ridge running to and from the dentine horn and some located centrally and towards the occlusal basin of the tooth crown. This feature may be linked to 'centrally placed cusps' noted at the OES of Neanderthal molars by others (Tattersall and Schwartz, 1999; Bailey, 2004). The range of variation in this feature is illustrated in Figure 2 and was scored as present (i.e., centrally placed) if the dentine horn tip exhibited any degree of central positioning relative to the marginal ridge. For the purpose of statistical analyses, counts for each mandibular and maxillary dentine horn included all three molar positions. Using Fisher's Exact Test (Fisher, 1922), the frequency of this trait for each dentine horn was compared between taxa (Neanderthals vs. recent modern humans and the earlier Neanderthal sample vs. the later Neanderthal sample). For obvious reasons, dentine horns that were reconstructed for the GM analysis were not included when evaluating this trait.

Post-paracone tubercle A number of maxillary molars present what we have decided to term a post-paracone tubercle. This manifests as a protuberance on the distal marginal ridge of the paracone. The degree of expression of this trait (Figure 3) was scored as absent, minor (ranging from a slight 'shouldering' of the ridge to a little less than a horizontal ridge feature), intermediate (a near horizontal ridge feature), or marked (a small dentine horn-like feature is present). A potentially developmentally similar feature was noted by Skinner et al. (2008c) on the distal marginal ridge of the metaconid dentine horn of mandibular molars and referred to at the OES in the cusp 7 ASUDAS description (Type 1A) as a post-metaconulid (Grine, 1981; Turner et al., 1991; Scott and Turner, 1997). Hershkovitz (1971) refers to an eoconule that is positioned distal to the eocone (a.k.a. paracone) in early therian mammals. However, given a lack of certainty as to the developmental homology of an eoconule to the trait found on hominin teeth, and the fact that a 'paraconule', being

a conule associated with the paracone, can be located either mesial or distal to the paracone, we are of the opinion that the most appropriate term for this feature is a post-paracone tubercle.

Crista obliqua The crista obliqua is a crest that courses obliquely across the occlusal surface of the maxillary molars. In addition to absence of expression, Sakai and Hanamura (1971) describe two types of crista obliqua. Type I being a crest between the lingual marginal ridge and the metacone and Type II being a crest between the protocone and metacone. In this paper, we describe and report the frequency of six types of crista obliqua expression (Figure 4). These six types of crista obliqua expression are: 1) a crest between the lingual marginal ridge distal to the protocone and the metacone dentine horn tip (like Type I of Sakai and Hanamura), 2) a crest between the tip of the protocone and metacone dentine horns (like Type II of Sakai and Hanamura), 3) a crest between the lingual marginal ridge distal to the protocone and the distal marginal ridge between the metacone and hypocone, 4) a crest between the tip of the protocone dentine horn and the distal marginal ridge between the metacone and hypocone (note: a dentine horn can be present at this location on the distal marginal ridge although it cannot be confidently attributed to a cusp 5 in all cases), 5) a crest between the lingual marginal ridge distal to the protocone and the metacone dentine horn tip and an additional crest from this crest to the distal marginal ridge between the metacone and hypocone, and 6) a crest between the tip of the protocone and metacone dentine horns and an additional crest from this crest to the distal marginal ridge between the metacone and hypocone.

Dentine horn patterning on the distal marginal ridge There are a number of crown features that can contribute to the morphology of the distal maxillary molar crown including the metacone and hypocone cusps, the distal marginal ridge, crista obliqua, and a cusp 5. Based on our preliminary observations of the distal marginal ridge of the EDJ in our Neanderthal sample, it became clear that it would be impossible to classify the variation in these features using traditional cusp nomenclature and/or the ASUDAS cusp 5 trait. Thus, we report on morphological variation on the distal marginal

ridge of the EDJ including the relative contribution of these features and then discuss the implications of this variation for characterising traits on the distal margin of the maxillary molar crown.

Twinned dentine horns A number of Neanderthal molars in the study sample exhibit EDJ dentine horns at the tip of which are not one, but two, small projections. To our knowledge this phenomenon has not been previously reported in the literature. We report on its prevalence in our Neanderthal sample and discuss how such features can be explained within current models of tooth cusp development.

Results

In the following section we report patterns of shape variation in EDJ ridge/CEJ ridge and CEJ ridge only analyses using PCAs and visualisations of shape differences between taxa (i.e., Neanderthals vs recent modern humans and the earlier Neanderthal sample vs. the later Neanderthal sample) and within taxa along the molar row (metameric variation) using wire frame models of the EDJ and CEJ ridges.

Mandibular first molar

Figure 5 shows the PCA plots of the EDJ/CEJ and CEJ analysis of the mandibular molars in shape space. In the EDJ/CEJ shape analysis for the M_1s, the earlier and the later Neanderthal samples are separate from the recent modern human sample, which exhibits relatively greater shape variation. There is greater overlap between taxa in the CEJ analysis with the later Neanderthal sample positioned between recent modern humans and the earlier Neanderthal sample. Examination of mean shape wire frame models highlights average EDJ/CEJ shape differences between recent modern humans and Neanderthals and between the earlier and the later Neanderthal sample (Figure 6). For example, comparing Neanderthals to the recent modern

humans, the metaconid is more centrally placed, the protoconid and hypoconid are closer together, the marginal ridge of the EDJ is larger relative to the CEJ, and the mesiobuccal corner of the CEJ is more centrally placed. In the later Neanderthal sample, compared to the earlier Neanderthal sample, the protoconid is shorter, the lingual marginal ridge of the EDJ has a shallow mandibular basin, and the entoconid is less centrally placed. The shape of the CEJ is similar between the two samples.

Mandibular second molar

In the EDJ/CEJ shape PCA for the M_2s, there is general separation between recent modern humans and early and late Neanderthals with the greatest variation exhibited by modern humans. In the CEJ analysis, there is separation between the earlier Neanderthal sample and the recent modern human sample with the later Neanderthal sample positioned intermediate. Comparing Neanderthals to recent modern humans, the metaconid is more centrally placed, the marginal ridge of the EDJ is mesiodistally stretched, and the CEJ is more rounded, which indents at the midpoints of the buccal and lingual faces in recent modern humans (Figure 6). In the later Neanderthal sample relative to the earlier Neanderthal sample, the entoconid and hypoconid are shorter and there are slight deviations in the mean shape of the cervix.

Mandibular third molar

In the EDJ/CEJ shape PCA for the M_3s, there is substantial overlap between the later Neanderthal sample and recent modern human sample and both overlap slightly with the earlier Neanderthal sample, which exhibits greater shape variation. In the CEJ analysis, there is considerable overlap between taxa indicating overall similarity in CEJ shape. Comparing Neanderthals to the recent modern humans, the metaconid and entoconid are more centrally placed, the protoconid is relatively tall, and the CEJ is more rounded, which indents at the midpoints of the buccal and lingual faces in recent modern humans (Figure 6). In the later Neanderthal sample relative to the earlier

Neanderthal sample, the positioning of each dentine horn is slightly different (particularly for the hypoconid) with earlier Neanderthals tending to have more centrally positioned dentine horn tips. The protoconid is relatively short in later Neanderthals and the distobuccal corner of the cervix is higher and less expanded.

Maxillary first molar

Figure 7 shows the PCA plots of the EDJ/CEJ and CEJ analysis of the maxillary molars in shape space. In both the EDJ/CEJ and CEJ shape analysis for the M^1s, taxa are well separated. Comparing Neanderthals to recent modern humans, the paracone is relatively short and more centrally placed, the hypocone is more centrally placed, and the distal marginal ridge is relatively low. The distolingual corner of the CEJ projects distolingually (Figure 8). Compared to the later Neanderthal sample, the earlier Neanderthal sample is distinguished by a less steeply sloping distal ridge of the paracone and a taller and more centrally positioned hypocone. The protocone and metacone are also closer together in the earlier Neanderthal sample, making the tooth more skewed in occlusal view. The distolingual corner of the CEJ projects slightly more in the earlier Neanderthal sample, and there is more of an indentation lingually.

Maxillary second molar

In the EDJ/CEJ shape PCA for the M^2s, there is overlap between all taxa, and the recent modern human sample exhibits considerable shape variation. In the CEJ analysis, there is greater overlap between taxa and more similar degrees of variation. Krapina D176 is an earlier Neanderthal and groups more closely with the recent modern humans due to a markedly reduced hypocone. It is excluded from the convex hull of the earlier Neanderthal sample to show that Neanderthals largely group on one end of PC1, while recent modern humans group on the other side (Figure 7). Comparing Neanderthals to recent modern humans, the protocone and metacone are closer together, and the paracone and hypocone are further apart, making the Neanderthal more skewed

(Figure 8). The CEJ of Neanderthals lacks the distal indentation seen in the CEJ of the recent modern humans. The protocone and paracone are closer together in the earlier Neanderthal sample relative to the later Neanderthal sample, making the earlier Neanderthal sample more skewed; and the CEJ is larger relative to the marginal ridge of the EDJ in the later Neanderthal sample than in the earlier Neanderthal sample.

Maxillary third molar

In both the EDJ/CEJ and CEJ shape PCAs for the M^3s, there is general separation between taxa. The Neanderthal M^3 appears more skewed than in recent modern humans, but this is due more to the mesial marginal ridge projecting mesially near the paracone than to the placement of the tips of the dentine horns (Figure 8). However, the metacone is still placed mesiolingually, and the hypocone is placed distolingually relative to recent modern humans. The CEJ of Neanderthals is relatively larger and is buccolingually longer relative to that of recent modern humans. Within the Neanderthal sample, both the paracone and hypocone are relatively short in the later Neanderthal sample relative to the earlier Neanderthal sample, while the metacone is relatively tall and more mesially placed. Also, the distolingual corner and the mesiobuccal corner of the EDJ are further apart in the later Neanderthal sample, making the CEJ more skewed.

Metameric variation

Metameric variation of EDJ/CEJ shape along the mandibular and maxillary molar rows can be assessed in each species through visual comparison of the mean shape at each molar position (Figure 9). In Neanderthal mandibular molars, there is a reduction in dentine horn height from M_1 to M_3 for each cusp. This reduction is most pronounced in the entoconid, hypoconid and hypoconulid. The dentine horn tips also become more centrally placed, being most pronounced in the protoconid and entoconid. This coincides with a general contraction of the EDJ marginal ridge relative to the cervix when viewed occlusally (not shown). Relative to the M_2 and M_3, the lingual margin of the M_1

cervix is slightly invaginated. Recent modern human mandibular molars exhibit a similar reduction in dentine horn height along the molar row. The most variable dentine horn in terms of relative height and placement is the hypoconid. The hypoconid is more distally placed but only slightly reduced in the M_2, and more mesially placed and markedly reduced in the M_3. Although not as marked as in Neanderthals, there is a trend towards more centrally placed dentine horns and contraction of the marginal ridge when moving distally from M_1 to M_3. The CEJ of the M_3 is superior to the M_2 and M_1 on the buccal side and the invagination of the CEJ outline on the buccal and lingual margins becomes less pronounced from M_1 to M_3.

For the maxillary molars of Neanderthals, the dentine horn height decreases from M^1 to M^3; particularly for the metacone and hypocone. Moving distally along the molar row, the marginal ridge of the EDJ become mesiodistally shorter, the shape of the tooth becomes less skewed as the paracone moves lingually, and the distolingual corner of the CEJ moves mesiobuccally. In recent modern humans, the dentine horns are shorter in the M^2 and M^3 relative to the M^1. In the M^3 (particularly for the metacone and hypocone), the marginal ridge between the metacone and hypocone is tall, relative to the M^1 and M^2. The shape of the molar also appears to become less skewed and the marginal ridge of the EDJ becomes mesiodistally shorter from M^1 to M^3. The CEJ become larger relative to the marginal ridge of the EDJ and more rounded moving down the molar gradient from the M^1 to the M^3.

CVA classification accuracy

The classification accuracies from the CVA of the mandibular molars are shown in Table 3 (recent modern humans and Neanderthals) and Table 4 (Neanderthals split into earlier and later samples). Neanderthals can be effectively discriminated from recent modern humans in both shape space and form space at both the CEJ and at the EDJ and CEJ combined at every molar position (with the exception of the CEJ in form space of the M_3, where Neanderthal specimens are correctly classified as Neanderthals only 78% of the time). When the Neanderthal specimens are split into

earlier and later Neanderthal samples overall classification success remains high, with accuracy falling below 80% in the earlier Neanderthal sample in shape space at the EDJ/CEJ of the M_3, and in form space at the CEJ of the M_2. The classification accuracy falls below 80% in the later Neanderthal sample in form space at the CEJ of the M_2.

The classification accuracies from the CVA of maxillary molars are shown in Table 5 (recent modern humans and Neanderthals) and Table 6 (Neanderthals split into earlier and later samples). Neanderthal maxillary molars can be effectively discriminated from recent modern human maxillary molars in both shape space and form space at both the CEJ and at the EDJ and CEJ combined at every molar position. When the Neanderthal specimens are split into earlier and later samples, accuracy falls below 80% in the later Neanderthal sample in form space at the CEJ of the M^2. Overall, these high classifications indicate a strong taxonomic signal in EDJ ridge and cervix shape.

Molar size

A boxplot showing the natural logarithm of molar centroid size with the sample divided by molar position and taxon is presented in Figure 10. Between group pairwise comparisons of centroid size are shown in Table 7 and within group pairwise comparisons are shown in Table 8. At each position, Neanderthal molars are significantly larger than the recent modern human molars, but there is not a significant difference in the size of the molars between the earlier and the later Neanderthal samples. Down the molar gradient, Neanderthal M^1/M_1s and Neanderthal M^2/M_2s (respectively) do not differ significantly in size, but both Neanderthal M^1/M_1s and Neanderthal M^2/M_2s are significantly larger than Neanderthal M^3/M_3s, respectively. In this analysis, recent modern human M_1s are significantly larger than recent modern human M_3s, but recent modern human M_2s are not significantly different in size to either M_1s or M_3s. Recent modern human M^1s are significantly larger than recent modern human M^2s and recent modern human M^3s, but recent modern human M^2s and recent modern human M^3s do not significantly differ in size. In recent modern human molars, the M^1/M_1 is always largest, followed by the M^2/M_2 and M^3/M_3. In both

Neanderthal samples, the molar size gradient tends to be $M_1<M_2>M_3$. In the maxillary molars, the earlier Neanderthal sample shares the recent modern human pattern $M^1>M^2>M^3$, while the later Neanderthal sample pattern is $M^1<M^2>M^3$.

Non-metric traits

Centrally placed dentine horns The frequency of centrally placed dentine horns by cusp is listed for the mandibular and maxillary molars in Table 9 and illustrated in Figure 11. On the mandibular molars, Neanderthals have significantly more centrally placed dentine horns on the metaconid ($p < 0.001$) and entoconid ($p < 0.01$) than recent modern humans. There is a significant difference in the frequency of centrally placed dentine horns between the earlier and the later Neanderthal samples on the protoconid ($p < 0.05$). On the maxillary molars, there is not a significant difference in the frequency of centrally placed dentine horns between Neanderthals and recent modern humans. However, the earlier Neanderthal sample specimens have more centrally placed dentine horns on the metacone than the later Neanderthal sample specimens ($p < 0.001$).

Post-paracone tubercle All Neanderthal maxillary molars (and many of the recent modern humans) included in this study exhibit at least some degree of expression of a post-paracone tubercle (Table 10). In Neanderthals, the trait tends to be more pronounced in the M^1s, with a majority of teeth expressing an intermediate form of the tubercle, compared to either the M^2s or the M^3s (whose predominant expression is minor). Although the sample size is small, the opposite pattern is present in the recent modern human sample with the M^3s expressing cases of intermediate and marked expression and the M^2s and M^1s dominated by minor expression.

Crista obliqua Variation in the patterning of the crista obliqua of the maxillary molars is shown in Figure 4 and frequencies of crista obliqua expression by type, taxa, and molar position are listed in Table 11. In Neanderthals, the M^1s typically exhibit the crista obliqua between the metacone and the

lingual marginal ridge (Type I), the M^2s typically between the protocone and metacone pattern (Type II), and the M^3s typically between the lingual marginal ridge and the distal marginal ridge (Type III). The other crista obliqua types occurred much more rarely. The recent modern human M^1 sample is dominated by Type I, while the M^2 sample is variable with three-quarters of the specimens expressing Type I or Type II, but also cases of absent expression and some cases of Type V and VI. The M^3 sample contains seven specimens, three of which have no crista obliqua expression, with one each of Types II and IV, and two of Type III.

Distal cusp patterning Neanderthal maxillary molars were observed to be highly variable in the patterning of their distal cusps, particularly in the M^3s, where there are nearly as many variants as there are specimens (Figure 12). For example, Krapina D97 M^3 exhibits a very reduced hypocone dentine horn and no marginal ridge running from the hypocone to either the crista obliqua or protocone. Krapina D173 M^3 exhibits a dentine horn distal to the metacone as well as a potential incipient dentine horn directly distal on the marginal ridge and a small dentine horn at the junction between the distal hypocone ridge and distal ridge (or crista obliqua). This is in addition to a diminutive hypocone with crests running towards the protocone and towards the distal marginal ridge. Similarly, Abri Bourgeois-Delaunay BD8 M^3 exhibits a hypocone similar to that in Krapina D97 M^3 (although with a more prominent dentine horn) and a similar dentine horn on the crista obliqua (at the point where a small crest joins from the hypocone). El Sidrón SD1164 M^3 has a large hypocone and exhibits a prominent dentine horn in the middle of the distal marginal ridge (notably there is a separate crista obliqua on this specimen) as well as an additional dentine horn distal to the metacone. El Sidrón SD621 exhibits a dentine horn distal to the metacone but with a distal ridge that does not join the distal marginal ridge (ending distally in a furrow). Mesial to this is a dentine horn at the end of what might be classified as either a crista obliqua or distal marginal ridge, and there is an additional dentine horn buccal to the hypocone on the distal hypocone ridge. Scladina 4A-3 M^2

exhibits a prominent dentine horn distobuccally to the hypocone. The interpretation of this variation with respect to the cusp 5 trait of the ASUDAS is discussed below.

In two Neanderthal mandibular second molars (one from the earlier Neanderthal sample and one from the later Neanderthal sample), there are examples of dentine horns between the hypoconid and hypoconulid. In both cases, there is no clear expression of this trait on the OES. However, the apparent absence of this trait at the OES could be the result of considerable enamel wear in both specimens. This trait was not observed in any of the recent modern human molars in the sample and this feature cannot be currently classified under the ASUDAS and is discussed further below.

Twinned dentine horns In the Neanderthal sample, both maxillary and mandibular molars can exhibit what we have termed twinned dentine horns (Figure 13 and SOM). In most cases, the two dentine horns are similar in size and shape and are present near the apex of the dentine horn and in line with the marginal ridge. In some specimens, two clearly protruding and isolated dentine horns are not present, but the unusually wide shape of the hypoconid dentine horn could indicate a diminutive form of this trait. In the mandibular molars of the earlier Neanderthal sample, the twinned dentine horn trait occurred on the hypoconid of the M_1 in five specimens. In the mandibular molars of the later Neanderthal sample, the twinned dentine horn trait occurred on the hypoconulid of the M_1 in one specimen. In the maxillary molars of the earlier Neanderthal sample, the twinned dentine horn trait occurred on the protocone of the M^1 in one specimen, on the metacone of the M^1 in one specimen, on the hypocone of the M^1 in three specimens, and on the fifth cusp of the M^3 in one specimen. In the maxillary molars of the later Neanderthal sample, the twinned dentine horn trait occurred on the metacone of the M^1 in one specimen, on the hypocone of the M^1 in one specimen, and on the metacone of the M^3 in one specimen.

Discussion

Neanderthals compared to recent modern humans

The results of this study show that the shape of the EDJ marginal ridge and the cervix of molars contain information helpful for discriminating Neanderthals from recent modern humans. These results are consistent with (and exceed in terms of classification accuracy) previous morphometric studies (Bailey, 2004; Gómez-Robles et al., 2007, 2012; Benazzi et al., 2011a), and studies focusing on the frequency and expression of non-metric traits (Bailey, 2002, 2006), which have shown Neanderthal permanent dental morphology to be distinct from recent modern humans. Previous geometric morphometric studies of the Neanderthal M^2 and the Neanderthal M^3 have yielded weak classification accuracy (Gómez-Robles et al., 2012), whereas the results of this study indicated very reliable classification accuracy in both form space and shape space for both the M^2 and the M^3 (see Table 5). Our results are also consistent with those of Benazzi et al. (2011a) in terms of classification accuracy of M^1/M_1 based on the cervix, suggesting that heavily worn molars can still have a reliable chance of accurate classification. The increased classification accuracy using EDJ/CEJ morphology found in this study compared to those based on the enamel surface is likely due to the inclusion of the vertical dimension (compared to 2D studies), which contributes taxonomically relevant shape information of relative dentine horn height and crown height.

With regard to crown shape differences between Neanderthals and recent modern humans, previous geometric morphometric studies of Neanderthal permanent molars have largely focused on the maxillary molars (Bailey, 2004; Gómez-Robles et al., 2007, 2012; Benazzi et al., 2011a). The M^1 of Neanderthals has previously been described as being markedly skewed relative to recent modern humans, having a narrower distal segment of the occlusal polygon in comparison to the mesial segment, a significantly larger hypocone, a significantly smaller metacone, and a smaller occlusal polygon, which reflects their centrally placed cusps (Bailey, 2004). This study focused on the EDJ, and did not examine relative cusp size, but the mean shape wireframe depicts a distolingual extension of the distolingual corner of the CEJ that would be consistent with an enlarged hypocone on the M^1, and our observations of centrally placed dentine horns is consistent with previous findings that

Neanderthals have centrally placed cusps and a smaller occlusal surface than recent modern humans (Tattersall and Schwartz, 1999; Bailey, 2004). The M^2 and M^3 of Neanderthals can both be described as more skewed than those of recent modern humans, but less dramatically than at the M^1. There is some degree of variation in hypocone development in the Neanderthal M^2s and M^3s and this may explain why such an 'elaborated' hypocone is not immediately obvious in the comparison of the Neanderthal and recent modern human mean models. Moving down the tooth row from the M^1 to the M^3 the distolingual extension of the distolingual corner of the CEJ becomes less pronounced, consistent with previous observations that the hypocone decreases in size down the molar gradient (Gómez-Robles et al., 2012).

The recent modern human sample used in this study presents two limitations for fully characterising the degree of distinctiveness of Neanderthal molars. First, our recent modern human sample is geographically limited (predominantly consisting of Europeans), and second, we do not include any fossil modern humans in this study. Future studies of EDJ morphology should include fossil *Homo sapiens* (e.g., Bailey, 2006) in order to determine whether particular aspects of Neanderthal crown size and shape, as well as the presence and degree of expression of particular dental traits, are derived or rather reflective of marked recent temporal changes in recent modern human molars. Similarly, given evidence for Neanderthal introgression into Upper Palaeolithic modern human samples (e.g., Fu et al., 2016), future analysis of such samples would require acknowledgment of the possibility that dental characteristics of Neanderthals may be present in a subsample of fossil modern human samples.

Temporal trends in Neanderthal molar morphology

The results of this study demonstrate that EDJ shape (including the cervix) effectively distinguishes between the earlier and the later Neanderthal samples at all molar positions, except the M^3, where classification accuracy falls to 71%. The cervix in isolation is less effective at discriminating between the earlier and the later Neanderthal samples but classification still remains

high with most analysis correctly classifying specimens >80% of the time. The reduced reliability of classification of the more distal molars is likely linked to their high variability and in particular to the variation in dentine horn patterning on the distal margin of the M^3. These findings are consistent with previous analyses of Neanderthal dental remains that found metric differences (particularly in the relative size of anterior and posterior teeth) between earlier and later samples (Wolpoff, 1979). These findings are also consistent with evolutionary models that incorporate temporal changes in Neanderthal morphology (e.g., Hublin, 2009; Bermúdez de Castro and Martinón-Torres, 2013). An important limitation to this study is that the earlier Neanderthal sample is dominated by specimens from Krapina, Croatia, with 23/30 mandibular molars and 33/36 maxillary molars EDJ/CEJ analyses coming from this site. The Scladina specimens, which are the oldest of the later Neanderthal sample (dating to MIS5c), classify to the later Neanderthal sample; however, a determination that it is not simply the distinctiveness of the Krapina population that is driving this result would be strengthened by the inclusion of additional pre-MIS5e samples. For example, the Neanderthal material from Sima de los Huesos would be ideal for providing information about whether the traits observed in the earlier Neanderthal sample are primitive relative to the later Neanderthal sample. As deduced by Weaver et al. (2007) from craniometric analysis, morphological changes within Neanderthal groups over time might have been largely driven by drift and one should highlight that ancestral change within modern humans witnessed similar changes (Vandermeersch 1981; Weaver et al., 2007; Bailey et al., in press). Interestingly, paleogenetic data indicate a last common ancestor of the last Neanderthals within MIS6 after a strong demographic reduction between 400 and 150 ka (Kuhlwilm et al., 2016) and without subsequent separation of Eastern and Western groups (Rougier et al., 2016; contra Fabre et al., 2009).

CVA classification accuracy

Generally speaking, inclusion of the shape of the EDJ ridge improves classification accuracy over just using the cervix. Exceptions to this general rule were found in this study. However, these

can be attributed to small samples sizes (e.g., Neanderthal M^3/M_3s) and/or the highly variable distal ridge of Neanderthal third molars (particularly the maxillary molars as presented in Figure 12).There is not a substantial difference in the classification accuracy between the mandibular and maxillary molars. It is usually in the CEJ ridge analyses that we see a greater difference in classification accuracy between mandibular and maxillary molars, and there is no consistency with regard to either the mandibular or maxillary molars classifying better than the other. Including size does not seem to improve classification accuracy in any consistent manner either. It is usually in the CEJ ridge analyses that we see a greater difference in classification accuracy between form space and shape space, and there is no consistency as to whether form space or shape space is providing greater classification accuracy. Classification accuracy tends to be higher in the M^1/M_1, than in the M^2/M_2 and M^3/M_3. This becomes more apparent when the Neanderthal sample is split into the earlier and the later Neanderthal samples. This is consistent with previous observations that have found M^1s to be more stable in their morphology than the other permanent molar types (Butler, 1963), thus M^1s should be expected to be more effective at discriminating between the earlier and the later Neanderthal samples than the M^2 or M^3. This pattern also holds for the mandibular molars.

Non-metric traits

Dental traits have served an important role in the study of taxonomy and phylogeny of other primates, both extant (Johanson, 1974; Uchida, 1998; Pilbrow, 2003) and extinct (Rosenberger and Delson, 1985; Gingerich et al., 1991; Pilbrow, 2006), and extinct hominins (Weidenreich, 1937; Robinson, 1956; Johanson and White, 1979; Wood and Abbott, 1983; Skelton and McHenry, 1986; Suwa et al., 1994; Bailey, 2002, 2006; Hlusko, 2004; Bailey and Lynch, 2005; Martinón-Torres et al., 2007; Irish et al., 2013). The ASUDAS system has standardised these traits for recent modern humans (Turner et al., 1991) and has been demonstrated to be effective in studying fossil hominins (Stringer et al., 1997; Irish, 1998; Tyrrell and Chamberlain, 1998; Bailey, 2000, 2002; Martinón-Torres et al., 2007; Irish et al., 2013). Examination of EDJ expression of dental traits elucidates their

development, improves the partitioning of their expression into morphological grades, and clarifies their presence and degree of expression in partially worn tooth crowns that can be used in the taxonomic assessment of fossil teeth (Skinner, 2008; Skinner et al., 2008c, 2009b; Bailey et al., 2011, Ortiz et al., 2012).

The EDJ expression of dental traits studied in our Neanderthal sample has highlighted considerable variation, with implications for understanding the developmental basis of these traits, as well as necessitating re-examination of how they might be studied under an ASUDAS-like system. For example, the post-paracone tubercle trait observed at the EDJ is not included in ASUDAS, and to our knowledge has never been explicitly described. A similar feature was noted distal to the metaconid at the EDJ of mandibular molars by Skinner et al. (2008c), who suggested that it is not homologous with a cusp 7 forming between the metaconid and entoconid. Developmentally, the presence of a dentine horn would suggest the presence of a secondary enamel knot during the development of the crown. The presence of similar dentine horns on the distal shoulder of the mesiolingual cusp of maxillary and mandibular molars would suggest that this trait should not be classified as a 'metaconulid-type' cusp 7 (contra Skinner et al., 2008c) but should be named for the maxillary and mandibular molars as a post-paracone tubercle and a post-metaconid tubercle, respectively. The marked degree of expression present in El Sidrón SD1164 might relate to the relatively long distal ridge of the paracone in this specimen (indicative of a location on the ridge far-removed from the paracone dentine horn where an additional enamel knot could be initiated). In addition to the influence of dentine horn spacing, future studies should examine the influence of the size of the paracone on the presence and degree of expression of the post-paracone tubercle, because both factors seem to be related to the expression of a cusp 6 in chimpanzees (Skinner and Gunz, 2010).

The crista obliqua is not included as a trait in ASUDAS and this study found considerable variation in this feature suggesting 1) that it could be useful as a non-metric dental trait for hominin systematics, and 2) that it will require its own definition and grading system. The main source of

variation in this feature seems to be whether a ridge running centrally from the metacone dentine horn tip is present in addition to a distal ridge from the metacone that normally contributes to the distal marginal ridge. This metacone central ridge can run directly to the paracone dentine horn tip or meet a ridge running distally from the paracone dentine horn. Complexity also arises from this distal ridge of the paracone as it can 1) meet a ridge running from the metacone, 2) run distally to the distal marginal ridge, and or 3) run adjacent to a second (more lingual) ridge running from the distal paracone towards the hypocone. It is also unclear to what extent accessory dentine horns along the distal crown (see below) influence this variation in the presence and branching combinations of these ridges. Hershkovitz (1971) identifies the plagioconule as a cusp that is present on the crista obliqua in primitive therian mammals and it has been illustrated at the EDJ in *Notharctus* (Anemone et al., 2012). However, given the considerable variation of dentine horn presence in association with the crista obliqua, hypocone, and metacone in this study, and our view that this variation could be caused by somewhat random perturbations in the development of the tooth germ, we are hesitant at the moment to assume homology between cuspules on primitive mammal crowns and those identified in our Neanderthal sample.

Cusp 5 is a well-established trait in ASUDAS, being a cusp that is situated along the distal marginal ridge between the metacone and hypocone (Scott and Turner, 1997). Unfortunately, its current definition is not useful for scoring variation observed on the distal margin of the EDJ of Neanderthal maxillary molars. In cases when a single dentine horn is present between the metacone and hypocone it can variably appear 1) adjacent and seemingly developmentally linked to the metacone, 2) adjacent and seemingly developmentally linked to the hypocone, or 3) in association with a ridge running distally from the protocone. There are also a number of specimens that present at least two (and even three) dentine horns between the metacone and the hypocone. This phenomenon of accessory dentine horns being preferentially associated with particular primary dentine horns has been noted for examination of cusp 6 on mandibular molars (Skinner et al., 2008c; Skinner and Gunz, 2010) and the iterative formation of dentine horns (explaining the presence of 1-3

accessory dentine horns) is consistent with the PCM of cusp development (see below). Thus, the homologous status of accessory dentine horns on the distal margin of upper molars is questionable and will require careful classification in order to be used in an ASUDAS-like system.

Our results indicate that centrally placed dentine horn tips are common in Neanderthals and are likely related to previous observations of centrally placed cusps at the outer enamel surface that have been previously described in both the mandibular (Tattersall and Schwartz, 1999) and maxillary molars (Bailey, 2004) of Neanderthals. This trait is very common in Neanderthals occurring predominantly on the metaconid and entoconid of the mandibular molars (the lingual side), and on the paracone and metacone of the maxillary molars (the buccal side). This trait would have an effect on a variety of standard measurements taken from molars such as cusp angles and the area of the occlusal polygon. The manifestation of this trait at the EDJ demonstrates that a dentine horn tip can be centrally placed independently from the marginal ridge. The observations in this study show that dentine horns (and their tips) are not simple conical structures. This is demonstrated by variation observed in the manifestation of centrally placed dentine horns shown in Figure 2, and the observation of twinned dentine horns shown in Figure 13. Further examination of this morphology could elucidate the processes underlying cell proliferation at secondary enamel knots.

Patterning cascade model of development

As mentioned above, the variation in the expression of the post-paracone tubercle could be interpreted within a PCM framework with degree of expression being influenced by the height of the paracone and length of the distal ridge. There is also a very high variability in the number and location of dentine horns on the distal margin of the M^2 and M^3. This could be related to the decrease in the size of the metacone and hypocone (and their inferred zones of secondary enamel knot suppression) along the maxillary molar tooth row in Neanderthals (Gómez-Robles et al., 2007, 2012). The EDJ of the M^1, which has a relatively large metacone and hypocone, did not display any dentine horn formation along its distal marginal ridge. This pattern has also been observed at the

OES (Gómez-Robles et al., 2012) and is consistent with the findings of C6 variation in chimpanzees (Skinner and Gunz, 2010) in which the lack of a C6 tends to be associated with large and relatively closely spaced hypoconulid and entoconid dentine horns. However, some observations in this study are difficult to explain within the PCM of development, particularly the observation in the Neanderthal sample of twinned dentine horns. These occurred on the hypoconulid and hypoconid in a few mandibular molars, and on the hypocone, protocone, and metacone in a few maxillary molars. It is difficult to conceptualise how this phenomenon could occur under the PCM of development, because one of the dentine horn tips should inhibit the development of the other. There were also two cases of an accessory dentine horn appearing between the hypoconid and hypoconulid in the Neanderthals. This phenomenon is also difficult to explain under a PCM because zones of inhibition from the hypoconid and hypoconulid should prevent this dentine horn from developing.

Conclusion

The results of this study confirm that Neanderthals differ significantly from recent modern humans in their molar morphology, and that earlier Neanderthal molars (albeit predominately represented by Krapina) can be distinguished from later Neanderthal molars based on morphology. This study also explored a variety of non-metric traits, such as centrally placed dentine horns, the crista obliqua, cusp 5, and the post-paracone tubercle. Our Neanderthal sample has a higher frequency of centrally placed dentine horns than our recent modern human sample at the metaconid and entoconid of the lower molars. Based on our sample, the crista obliqua appears to be useful in determining molar position in Neanderthals, with the Type I variant being more commonly expressed in the M^1, the Type II variant being more commonly expressed in the M^2, and the Type III being more commonly expressed in the M^3. Cusp 5 was shown to be especially variable in the Neanderthal M^3. The post-paracone tubercle tends to be more prominently expressed in the M^1 of the Neanderthal sample than in in the M^2 or M^3, while the opposite pattern is present in the recent modern human sample with the trait being more prominently expressed in the M^3 than in the M^2 or

M^1. Observations of dentine horn patterning largely fit within the PCM of development. However, some features, such as the twinned dentine horn, and the accessory cusp between the hypoconid and hypoconulid are difficult to explain, and could indicate that tooth development is more complicated than previously thought. Further analyses of the changes of molar morphology in Neanderthals following the Eemian interglacial period demonstrated in this study would benefit from the inclusion of older Middle Pleistocene hominin specimens to assess the polarity of the different features (i.e., which features are primitive and which features are derived) between the earlier and the later Neanderthal samples.

Acknowledgments

For access to specimens, we thank Antonio Rosas (Museo Nacional de Ciencias Naturales), Flora Groening (Senckenberg, Forschungsstation für Quartärpaläontologie), Roberto Macchiarelli (The Neanderthal Tools Project of the Neanderthal Studies Professional Online Service), Michel Toussaint (ASBL Archéologie Andennaise, and Royal Belgian Institute of Natural Sciences), Jakov Radovčić (Croatian Natural History Museum), Dejana Brajković (Croatian Academy of Sciences and Arts), Jean-Jacques Cleyet-Merle (Musée National de la Préhistoire des Eyzies-de-Tayac), Yoel Rak, Alon Barash, Israel Hershkovitz (Sackler School of Medicine, Tel Aviv University), Jean-François Tournepiche (Musée d'Angoulême), Patrick Périn (Musée d'Archéologie nationale de Saint-Germain-en-Laye), Almut Hoffmann (Museum für Vor und Frühgeschichte Berlin), David Hunt (National Museum of Natural History), Andrei Dorian Soficaru ("Francisc J. Rainer" Institute of Anthropology), and Christine Feja (Universität Leipzig, Institut für Anatomie, Lehrsammlung Anatomie). For scanning assistance we thank Heiko Temming, Kornelius Kupczik, Tanya Smith, and Adeline Le Cabec.

References

Aiello, L., Dean, C. 2002. An Introduction to Human Evolutionary Anatomy. Academic Press, London.

Anemone, R.L., Skinner, M.M., Dirks, W., 2012. Are there two distinct types of hypocone in Eocene primates? The 'pseudohypocone' of notharctines revisited. Palaeontol Electron. 15, 26A, 13p.

Arsuaga, J.L., Martínez, I., Gracia, A., Lorenzo, C., 1997. The Sima de los Huesos crania (Sierra de Atapuerca, Spain). A comparative study. J. Hum. Evol. 33, 219–281.

Arsuaga, J.L., Martínez, I., Arnold, L.J., Aranburu, A., Gracia-Téllez, A., Sharp, W.D., Quam, R.M., Falguères, C., Pantoja-Pérez, A., Bischoff, J., Poza-Rey, E., Parés, J.M., Carretero, J.M., Demuro, M., Lorenzo, C., Sala, N., Martinón-Torres, M., García, N., Alcázar de Velasco, A., Cuenca-Bescós, G., Gómez-Olivencia, A., Moreno, D., Pablos, A., Shen, C.-C., Rodríguez, L., Ortega, A.I., García, R., Bonmatí, A., Bermúdez de Castro, J.M., Carbonell, E., 2014. Neandertal roots: ~~Cranial~~ cranial and chronological evidence from Sima de los Huesos. Science 344, 1358–1363.

Bailey, S.E., 2000. Dental morphological affinities among late Pleistocene and recent humans. Dent. Anthropol. 14, 1–8.

Bailey, S.E., 2002. A closer look at Neanderthal postcanine dental morphology: ~~The~~ the mandibular dentition. Anat. Rec. (New Anat.). 269, 148–156.

Bailey, S.E., 2004. A morphometric analysis of maxillary molar crowns of Middle-Late Pleistocene hominins. J. Hum. Evol. 47, 183–198.

Bailey, S.E., 2006. Beyond shovel-shaped incisors: Neandertal dental morphology in a comparative context. Period. Biol. 108, 253–267.

Bailey, S.E., Hublin, J.-J., 2006. Dental remains from the Grotte du Renne at Arcy-sur-Cure (Yonne). J. Hum. Evol. 50, 485–508.

Bailey, S.E., Lynch, J.M., 2005. Diagnostic differences in mandibular P4 shape between Neandertals and anatomically recent modern humans. Am. J. Phys. Anthropol. 126, 268–277.

Bailey, S.E., Skinner, M.M., Hublin, J.-J., 2011. What lies beneath? An evaluation of mandibular molar trigonid crest patterns based on both dentine and enamel expression. Am. J. Phys. Anthropol. 145, 505–518.

Bailey, S.E., Benazzi, S., Souday, C., Astorino, C., Paul, K., Hublin, J.-J., 2014. Taxonomic differences in deciduous maxillary second molar crown outlines of *Homo sapiens*, *Homo neanderthalensis* and *Homo erectus*. J. Hum. Evol. 72, 1–9.

Bailey, S.E., Weaver, T.D., Hublin, J.-J., In Press. The dentition of the earliest modern humans. How 'modern' are they? In: Marom, A., Hovers, E. (Eds.), Human Paleontology and Prehistory Contributions in Honor of Yoel Rak. Springer, New York.

Benazzi, S., Coquerelle, M., Fiorenza, L., Bookstein, F., Katina, S., Kullmer, O., 2011a. Comparison of dental measurement systems for taxonomic assignment of first molars. Am. J. Phys. Anthropol. 144, 342–354.

Benazzi, S., Fornai, C., Bayle, P., Coquerelle, M., Kullmer, O., Mallegni, F., Weber, G.W., 2011b. Comparison of dental measurement systems for taxonomic assignment of Neanderthal and recent modern human mandibular second deciduous molars. J. Hum. Evol. 61, 320–326.

Benazzi, S., Fornai, C., Buti, L., Toussaint, M., Mallegni, F., Ricci, S., Gruppioni, G., Weber, G.W., Condemi, S., Ronchitelli, A., 2012. Cervical and crown outline analysis of worn Neanderthal and recent modern human mandibular second deciduous molars. Am. J. Phys. Anthropol. 149, 537–546.

Bermúdez de Castro, J.M., Martinón-Torres, M., 2013. A new model for the evolution of the human Pleistocene populations of Europe. Quatern. Int. 295, 102–112.

Bermúdez de Castro, J.M., Rosas, A., Nicolás, M.E., 1999. Dental remains from Atapuerca-TD6 (Gran Dolina site, Burgos, Spain). J. Hum. Evol. 37, 523–566.

Blackwell, B., Schwarcz, H.P., 1986. U-Series analyses of the mandibular travertine at Ehringsdorf, DDR. Quatern. Res. 25, 215–222.

Comment [A1]: We do not have page numbers yet as it is in press

Blackwell, B., Schwarcz, H.P., Debénath, A., 1983. Absolute dating of hominids and palaeolithic artifacts of the cave of La Chaise-de-Vouthon (Charente), France. J. Archaeol. Sci. 10, 493–513.

Bookstein, F.L., 1991. Morphometric Tools for Landmark Data: Geometry and Biology. Cambridge University Press, Cambridge.

Bookstein, F.L., 1997. Landmark methods for forms without landmarks: ~~Morphometrics~~ morphometrics of group differences in outline shape. Med. Imag. Anal. 1, 225–243.

Braga, J., Thackeray, J.F., Subsol, G., Kahn, J.L., Maret, D., Treil, J., Beck, A., 2010. The enamel-dentine junction in the postcanine dentition of *Australopithecus africanus*: i~~I~~ntra-individual metameric and antimeric variation. J. Anat. 216, 62–79.

Butler, P.M., 1956. The ontogeny of molar pattern. Biol. Rev. 31, 30–69.

Butler, P.M., 1963. Tooth morphology and primate evolution. In: Brothwell, D.R. (Ed.), Dental Anthropology. Pergamon Press, New York, pp. 1-13.

Butler, P.M., 1999. The relation of cusp development and calcification to growth. In: Mayhall, J.T., Heikkinen, T. (Eds.), Proceedings of the 11th International Symposium on Dental Morphology, Oulu, Finland, 1998. Oulu University Press, Oulu, Finland, pp. 26–32.

Cavanhié, N., 2010. L'ours qui a vu l'homme? Étude archéozoologique et taphonomique du site paléolithipue moyen de Regourdou (Montignac, Dordogne, France). Paléo. 21, 39–64.

Condemi, S., 2001. 8-Les Dents – Les Néandertaliens de La Chaise (Abri Bourgeois-Delaunay). Editions du CTHS, Paris.

Corruccini, R.S., 1987. The dentinoenamel junction in primates. Int. J. Primatol. 8, 99–114.

Corruccini, R.S.,1998. The dentino-enamel junction in primate mandibular molars. In: Lukacs, J.R. (Ed.), Human Dental Development, Morphology, and Pathology: A Tribute to Albert A. Dahlberg. University of Oregon Anthropological Papers, Portland, pp. 1–16.

Dahl-Jensen, D., Albert, M.R., Aldahan, A., Azuma, N., Balslev-Clausen, D., Baumgartner, M., Berggren, A.-M., Bigler, M., Binder, T., Blunier, T., Bourgeois, J.C., Brook, E.J., Buchardt, S.L., Buizert, C., Capron, E., Chappellaz, J., Chung, J., Clausen, H.B., Cvijanovic, I., Davies, S.M.,

Ditlevsen, P., Eicher, O., Fischer, H., Fisher, D.A., Fleet, L.G., Gfeller, G., Gkinis, V., Gogineni, S., Goto-Azuma, K., Grinsted, A., Gudlaugsdottir, H., Guillevic, M., Hansen, S.B., Hansson, M., Hirabayashi, M., Hong, S., Hur, S.D., Huybrechts, P., Hvidberg, C.S., Iizuka, Y., Jenk, T., Johnsen, S.J., Jones, T.R., Jouzel, J., Karlsson, N.B., Kawamura, K., Keegan, K., Kettner, E., Kipfstuhl, S., Kjær, H.A., Koutnik, M., Kuramoto, T., Kohler, P., Laepple, T., Landais, A., Langen, P.L., Larsen, L.B., Leuenberger, D., Leuenberger, M., Leuschen, C., Li, J., Lipenkov, V., Martinerie, P., Maselli, O., Masson-Delmotte, V., McConnell, J.R., Miller, H., Mini, O., Miyamoto, A., Montagnat-Rentier, M., Mulvaney, R., Muscheler, R., Orsi, A.J., Paden, J., Panton, C., Pattyn, F., Petit, J.-R., Pol, K., Popp, T., Possnert, G., Prie, F., Prokopiou, M., Quiquet, A., Rasmussen, S.O., Raynaud, D., Ren, J., Reutenauer, C., Ritz, C., Rockmann, T., Rosen, J.L., Rubino, M., Rybak, O., Samyn, D., Sapart, C.J., Schilt, A., Schmidt, A.M.Z., Schwander, J., Schupbach, S., Seierstad, I., Severinghaus, J.P., Sheldon, S., Simonsen, S.B., Sjolte, J.~~Sheldon, J.~~, Solgaard, A.M., Sowers, T., Sperlich, P., Steen-Larsen, H.C., Steffen, K., Steffensen, J.P., Steinhage, D., Stocker, T.F., Stowasser, C., Sturevik, A.S., Sturges, W.T., Sveinbjornsdottir, A., Svensson, A., Tison, J.-L., Uetake, J., Vallelonga, P., van de Wal, R.S.W., van der Wel, G., Vaughn, B.H., Vinther, B., Waddington, E., Wegner, A., Weikusat, I., White, J.W.C., Wilhelms, F., Winstrup, M., Witrant, E., Wolff, E.W., Xiao, C., Zheng, J., 2013. Eemian interglacial reconstructed from a Greenland folded ice core. Nature 493, 489–494.

Delpech, F., 1996. L'environnement animal des Moustériens Quina du Périgord. Paléo. 8, 31–46.

Delson, E., Tattersall, I., Van Couvering, J.A., Brooks, A.S. (Eds.), 2000. Encyclopedia of Human Evolution and Prehistory. Garland Pub. Inc., New York.

Dennell, R.W., Martinón-Torres, M., Bermúdez de Castro, J.M., 2011. Hominin variability, climatic instability and population demography in Middle Pleistocene Europe. Quaternary Sci. Rev. 30, 1511–1524.

Dryden, I., Mardia, K.V., 1998. Statistical Shape Analysis. John Wiley and Sons, New York.

Ellwood, B.B., Harrold, F.B., Benoist, S.L., Thacker, P., Otte, M., Bonjean, D., Long, G.J., Shahin, A.M., Hermann, R.P., Grandjean, F., 2004. Magnetic susceptibility applied as an age–depth–climate relative dating technique using sediments from Scladina Cave, a Late Pleistocene cave site in Belgium. J. Archaeol. Sci. 31, 283–293.

Fabre, V., Condemi, S., Degioanni, A., 2009. Genetic evidence of geographical groups among Neanderthals. PLoS ONE 4, e5151.

Finlayson, C., Pacheco, F.G., Rodríguez-Vidal, J., Fa, D.A., Gutierrez López, J.M., Santiago Pérez, A., Finlayson, G., Allue, E., Baena Preysler, J., Cáceres, I., Carrión, J.S., Fernández Jalvo, Y., Gleed-Owen, C.P., Jimenez Espejo, F.J., López, P., López Sáez, J.A., Riquelme Cantal, J.A., Sánchez Marco, A., Guzman, F.G., Brown, K., Fuentes, N., Valarino, C.A., Villalpando, A., Stringer, C.B., Martinez Ruiz, F., Sakamoto, T., 2006. Late survival of Neanderthals at the southernmost extreme of Europe. Nature 443, 850–853.

Fisher, R.A., 1922. On the interpretation of χ2 from contingency tables, and the calculation of P. J. R. Stat. Soc. 85, 87–94.

Fu, Q., Hajdinjak, M., Moldovan, O.T., Constantin, S., Mallick, S., Skoglund, P., Patterson, N., Rohland, N., Lazaridis, I., Nickel, B., Viola, B., Prüfer, K., Meyer, M., Kelso, J., Riech, D., Pääbo, S., 2015. An early modern human from Romania with a recent Neanderthal ancestor. Nature 524, 216-219.

Garralda, M.-D., Vandermeersch, B., 2000. Les Néandertaliens de la grotte de Combe-Grenal (Domme, Dordogne, France) / The Neanderthals from Combe-Grenal cave (Domme, Dordogne, France). Paléo. 12, 213–259.

Gingerich, P.D., Dashzeveg, D., Russell, D.E., 1991. Dentition and systematic relationships of *Altanius orlovi* (Mammalia, Primates) from the ~~Earlier~~ earlier Eocene of Mongolia. Geobios. 24, 637–646.

Gómez-Robles, A., Martinón-Torres, M., Bermúdez de Castro, J.M., Margvelashvili, A., Bastir, M., Arsuaga, J.L., Pérez-Pérez, A., Estebaranz, F., Martínez, L.M., 2007. A geometric morphometric analysis of hominin maxillary first molar shape. J. Hum. Evol. 53, 272–285.

Gómez-Robles, A., Martinón-Torres, M., Bermúdez de Castro, J.M., Prado, L., Sarmiento, S., Arsuaga, J.L., 2008. Geometric morphometric analysis of the crown morphology of the mandibular first premolar of hominins, with special attention to Pleistocene *Homo*. J. Hum. Evol. 55, 627–638.

Gómez-Robles, A., Bermúdez de Castro, J.M., Martinón-Torres, M., Prado-Simón, L., Arsuaga, J.L., 2012. A geometric morphometric analysis of hominin maxillary second and third molars, with particular emphasis on European Pleistocene populations. J. Hum. Evol. 63, 512–526.

Goodall, C., 1991. Procrustes methods in the statistical analysis of shape. J. R. Stat. Soc. Series. B. Stat. Methodol. 53, 285–339.

Gower, J.C., 1975. Generalized Procrustes analysis. Psychometrika~~.~~ 40, 33–51.

Green, R.E., Krause, J., Briggs, A.W., Maricic, T., Stenzel, U., Kircher, M., Patterson, N., Li, H., Zhai, W., Fritz, M.H.-Y., Hansen, N.F., Durand, E.Y., Malaspinas, A.-S., Jensen, J.D., Marques-Bonet, T., Alkan, C., Prüfer, K., Meyer, M., Burbano, H.A., Good, J.M., Schultz, R., Aximu-Petri, A., Butthof, A., Höber, B., Höffner, B., Siegemund, M., Weihmann, A., Nusbaum, C., Lander, E.S., Russ, C., Novod, N., Affourtit, J., Egholm, M., Verna, C., Rudan, P., Brajkovic, D., Kucan, Z., Gusic, I., Doronichev, V.B., Golovanova, L.V, Lalueza-Fox, C., de la Rasilla, M., Fortea, J., Rosas, A., Schmitz, R.W., Johnson, P.L.F., Eichler, E.E., Falush, D., Birney, E., Mullikin, J.C., Slatkin, M., Nielsen, R., Kelso, J., Lachmann, M., Reich, D., Pääbo, S., 2010. A draft sequence of the Neandertal genome. Science 328, 710–722.

Grine, F.E., 1981. Trophic differences between gracile and robust australopithecines-a scanning electron-microscope analysis of occlusal events. S. Afr. J. Sci. 77, 203–230.

Guadelli, J.L., Laville, H., 1990. L'environnement climatique de la fin du Moustérien à Combe-Grenal et à Camiac. Confrontation des données naturalistes et impications. In: Farizy, C. (Ed.), Paléolithique moyen récent et Paléolithique supérieur ancien en Europe. Mem. du Musée de Préhistoire d'Ile de France, Nemours, pp. 43–48.

Guatelli-Steinberg, D., Irish, J.D., 2005. ~~Brief communication: Earlier earlier~~Earlier hominin variability in first molar dental trait frequencies. Am. J. Phys. Anthropol. 128, 477–484.

Guérin, G., Discamps, E., Lahaye, C., Mercier, N., Guibert, P., Turq, A., Dibble, H.L., McPherron, S.P., Sandgathe, D., Goldberg, P., Jain, M., Thomsen, K., Patou-Mathis, M., Castel, J.-C., Soulier, M.-C., 2012. Multi-method (TL and OSL), multi-material (quartz and flint) dating of the Mousterian site of Roc de Marsal (Dordogne, France): ~~Correlating~~ correlating Neanderthal occupations with the climatic variability of MIS 5–3. J. Archaeol. Sci. 39, 3071–3084.

Gunz, P., Mitteroecker, P., 2013. Semilandmarks: ~~A~~ a method for quantifying curves and surfaces. It. J. Mammal. 24, 103–109.

Gunz, P., Mitteroecker, P., Bookstein, F.L., 2005. Semilandmarks in three dimensions. In: Slice, D. (Ed.), Recent Modern Morphometrics in Physical Anthropology. Kluwer Academic/Plenum Publishers, New York, pp. 73–98.

Hair, J.F., Anderson, R.E., Tatham R.I., Black W.C., 1998. Multivariate Data Analysis. Prentice Hall, New Jersey.

Harvati, K., Panagopoulou, E., Karkanas, P., 2003. First Neanderthal remains from Greece: ~~The~~ the evidence from Lakonis. J. Hum. Evol. 45, 465–473.

Hershkovitz, P., 1971. Basic crown patterns and cusp homologies of mammalian teeth. In: Dahlberg, A.A. (Ed.), Dental Morphology and Evolution. University of Chicago Press, Chicago, pp. 95–150.

Hlusko, L.J., 2004. Protostylid variation in *Australopithecus*. J. Hum. Evol. 46, 579–594.

Howell, F.C., 1960. European and Northwest African Middle Pleistocene hominids. Curr. Anthropol. 1, 195–232.

Hublin, J.-J., 1998. Climatic changes, paleogeography, and the evolution of the Neandertals. In: Akazawa, T., Aoki, K., Bar-Yosef, O. (Eds.), Neandertals and Modern Humans in Western Asia. Plenum Press, New York, pp. 295–310.

Hublin, J.-J., 2009. The origin of Neandertals. Proc. Natl. Acad. Sci. 106, 16022–16027.

Hublin, J.-J., Talamo, S., Julien, M., David, F., Connet, N., Bodu, P., Vandermeersch, B., Richards, M.P., 2012. Radiocarbon dates from the Grotte du Renne and Saint-Césaire support a Neandertal origin for the Châtelperronian. Proc. Natl. Acad. Sci. 109, 1–6.

Irish, J.D., 1998. Ancestral dental traits in recent Sub-Saharan Africans and the origins of recent modern humans. J. Hum. Evol. 34, 81–98.

Irish, J.D., Guatelli-Steinberg, D., Legge, S.S., 2013. Dental morphology and the phylogenetic "place" of *Australopithecus sediba*. Science 340, 1233062–1233064.

Jernvall, J., 2000. Linking development with generation of novelty in mammalian teeth. Proc. Natl. Acad. Sci. 97, 2641–2645.

Jernvall, J., Jung, H.-S., 2000. Genotype, phenotype, and developmental biology of molar tooth characters. Am. J. Phys. Anthropol. 43, 171–190.

Jernvall, J., Thesleff, I., 2000. Reiterative signaling and patterning during mammalian tooth morphogenesis. Mech. Dev. 92, 19–29.

Johanson, D.C., 1974. An ondontological study of chimpanzees with some implications for hominoid evolution. Ph.D. Dissertation, University of Chicago.

Johanson, D.C., White, T.D., 1979. A systematic assessment of ~~Earlier~~ earlier African hominids. Science 203, 321–330.

Kangas, A.T., Evans, A.R., Thesleff, I., Jernvall, J., 2004. Nonindependence of mammalian dental characters. Nature 432, 211–214.

Kassai, Y., Munne, P., Hotta, Y., Penttilä, E., Kavanagh, K., Ohbayashi, N., Takada, S., Thesleff, I., Jernvall, J., Itoh, N., 2005. Regulation of mammalian tooth cusp patterning by ectodin. Science 309, 2067–2070.

Korenhof, C.A.W., 1961. The enamel-dentine border: ~~A~~ a new morphological factor in the study of the (human) molar pattern. Proc. Koninkl. Nederl. Acad. Wetensch. 64, 639–664.

Korenhof, C.A.W., 1982. Evolutionary trends of the inner enamel anatomy of deciduous molars from Sangiran (Java, Indonesia). In: Kurten, B. (Ed.), Teeth: Form, Function and Evolution. Columbia University Press, New York, pp. 350–365.

Kovarovic, K., Aiello, L.C., Cardini, A., Lockwood, C.A., 2011. Discriminant function analyses in archaeology: ~~Are~~ are classification rates too good to be true? J. Archaeol. Sci. 38, 3006–3018.

Kraus, B.S., 1952. Morphologic relationships between enamel and dentin surfaces of mandibular first molar teeth. J. Dent. Res. 31, 248–256.

Kraus, B.S., Jordan, R., 1965. The Human Dentition before Birth. Lea and Febiger, Philadelphia.

Kruskal, W.H., Wallis, W.A., 1952. Use of ranks in one-criterion variance analysis. J. Am. Statist. Assoc. 47, 583–621.

Kuhlwilm, M., Gronau, I., Hubisz, M.J., de Filippo, C., Prado-Martinez, J., Kircher, M., Fu, Q., Burbano, H.A., Lalueza-Fox, C., de la Rasilla, M., Rosas, A., Rudan, P., Brajkovic, D., Kucan, Z., Gušic, I., Marques-Bonet, T., Andrés, A.M., Viola, B., Pääbo, S., Meyer, M., Siepel, A., Castellano, S., 2016. Ancient gene flow from early modern humans into ~~Eastern~~ eastern Neanderthals. Nature 530, 429-433.

Macchiarelli, R., Bondioli, L., Debénath, A., Mazurier, A., Tournepiche, J.-F., Birch, W., Dean, C., 2006. How Neanderthal molar teeth grew. Nature 444, 748–751.

Martin, H., 1920. Présentation d'un crane d'enfant de 8 ans trouvé en place dans le moustérien de La Quina (Charente). Bull. Mém. Soc. Anthropol. Paris 1, 113–125.

Martínez de Pinillos, M., Martinón-Torres, M., Skinner, M.M., Arsuaga, J.L., Gracia-Téllez, A., Martínez, I., Martín-Francés, L., Bermúdez de Castro, J.M., 2014. Trigonid crests expression in Atapuerca-Sima de los Huesos mandibular molars: ~~Internal~~ internal and external morphological expression and evolutionary inferences. C. R. Palevol. 13, 205–221.

Martinón-Torres, M., Bastir, M., Bermúdez de Castro, J.M., Gómez, A., Sarmiento, S., Muela, A., Arsuaga, J.L., 2006. Hominin mandibular second premolar morphology: ~~Evolutionary~~ evolutionary inferences through geometric morphometric analysis. J. Hum. Evol. 50, 523–533.

Martinón-Torres, M., Bermúdez de Castro, J.M., Gómez-Robles, A., Arsuaga, J.L., Carbonell, E., Lordkipanidze, D., Manzi, G., Margvelashvili, A., 2007. Dental evidence on the hominin dispersals during the Pleistocene. Proc. Natl. Acad. Sci. 104, 13279–13282.

Martinón-Torres, M., Bermúdez de Castro, J.M., Gómez-Robles, A., Prado-Simón, L., Arsuaga, J.L., 2012. Morphological description and comparison of the dental remains from Atapuerca-Sima de los Huesos site (Spain). J. Hum. Evol. 62, 7–58.

Martinón-Torres, M., Spěváčková, P., Gracia-Téllez, A., Martínez, I., Bruner, E., Arsuaga, J.L., Bermúdez de Castro, J.M., 2013. Morphometric analysis of molars in a Middle Pleistocene population shows a mosaic of "recent modern" and Neanderthal features. J. Anat. 223, 353–363.

Martinón-Torres, M., Martínez de Pinillos, M., Skinner, M.M., Martín-Francés, L., Gracia-Téllez, A., Martínez, I., Arsuaga, J.L., Bermúdez de Castro, J.M., 2014. Talonid crests expression at the enamel–dentine junction of hominin mandibular permanent and deciduous molars. C. R. Palevol. 13, 223–234.

Mellars, P., Grün, R., 1991. A comparison of the electron spin resonance and thermoluminescence dating methods: the results of ESR dating at Le Moustier (France). Cambridge- Archaeol. J. 1, 269–276.

Mercier, N., 1992. Apport des méthodes de datation radionucléaires à l'étude du peuplement préhistorique de l'Europe et du Proche-Orient au cours du Pléistocène supérieur. Ph.D. Dissertation, Université de Bordeaux 1.

Mercier, N., Valladas, H., 1998. Datations. Gallia. Préhist. 40, 70–71.

Mercier, N., Valladas, H., Joron, J.-L., Reyss, J.-L., Lévêque, F., Vandermeersch, B., 1991. Thermoluminescence dating of the late Neanderthal remains from Saint-Césaire. Nature 351, 737–739.

Meyer, M., Kircher, M., Gansauge, M., Li, H., Racimo, F., Mallick, S., Schraiber, J.G., Jay, F., Prüfer, K., De Filippo, C., Sudmant, P.H., Alkan, C., Fu, Q., Do, R., Rohland, N., Tandon, A., Siebauer, M., Green, R.E., Bryc, K., Briggs, A.W., Stenzel, U., Dabney, J., Shendure, J., Kitzman, J., Hammer, M.F., Shunkov, M.V, Derevianko, A.P., Patterson, N., Andrés, A.M., Eichler, E.E., Slatkin, M.,

Reich, D., Kelso, J., Pääbo, S., 2012. A high-coverage genome sequence from an archaic Denisovan individual. Science 338, 222–227.

Meyer, M., Arsuaga, J.-L., de Filippo, C., Nagel, S., Aximu-Petri, A., Nickel, B., Martínez, I., Gracia, A., de Castro, J.M.B., Carbonell, E., Viola, B., Kelso, J., Prüfer, K., Pääbo, S., 2016. Nuclear DNA sequences from the Middle Pleistocene Sima de los Huesos hominins. Nature 531, 504–507.

Ortiz, A., Skinner, M.M., Bailey, S.E., Hublin, J.-J., 2012. Carabelli's trait revisited: ~~An~~ an examination of mesiolingual features at the enamel-dentine junction and enamel surface of *Pan* and *Homo sapiens* maxillary molars. J. Hum. Evol. 63, 586–596.

Pilbrow, V., 2006. Population systematics of chimpanzees using molar morphometrics. J. Hum. Evol. 51, 646–662.

Pilbrow, V.C., 2003. Dental variation in African apes with implications for understanding patterns of variation in species of fossil apes. Ph.D. Dissertation, New York University.

Pirson, S., Bonjean, D., Toussaint, M., 2014. Stratigraphic origin of the juvenile Neanderthal remains from Scladina Cave: ~~R~~re-evaluation and consequences for their palaeoenvironmental and chronostratigraphic contexts. In: Toussaint, M., Bonjean, D. (Eds.), The Scladina I-4A Juvenile Neandertal (Andenne, Belgium). Palaeoanthropology and Context, Liege, pp. 93–124.

Polly, P.D., 1998. Variability, selection, and constraints: ~~Development~~ development and evolution in viverravid (Carnivora, Mammalia) molar morphology. Paleobiol. 24, 409–429.

Prüfer, K., Racimo, F., Patterson, N., Jay, F., Sankararaman, S., Sawyer, S., Heinze, A., Renaud, G., Sudmant, P.H., de Filippo, C., Li, H., Mallick, S., Dannemann, M., Fu, Q., Kircher, M., Kuhlwilm, M., Lachmann, M., Meyer, M., Ongyerth, M., Siebauer, M., Theunert, C., Tandon, A., Moorjani, P., Pickrell, J., Mullikin, J.C., Vohr, S.H., Green, R.E., Hellmann, I., Johnson, P.L.F., Blanche, H., Cann, H., Kitzman, J.O., Shendure, J., Eichler, E.E., Lein, E.S., Bakken, T.E., Golovanova, L. V, Doronichev, V.B., Shunkov, M. V, Derevianko, A.P., Viola, B., Slatkin, M., Reich, D., Kelso, J.,

Pääbo, S., 2014. The complete genome sequence of a Neanderthal from the Altai mountains. Nature 505, 43–49.

Radovčić, J., Smith, F.H., Trinkaus, E., Wolpoff, M.H., 1988. The Krapina Hominids: An Illustrated Catalog of the Skeletal Collection. Mladost Publishing House, Zagreb.

Rink, W.J., Schwarcz, H.P., Smith, F.H., Radovčić, J., 1995. ESR ages for Krapina hominids. Nature 378, 24.

Robinson, J.T., 1956. The Dentition of the Australopithecinae, Transvaal Museum Memoir, vol. 9. The Transvaal Museum, Pretoria.

Rohlf, F.J., Slice, D., 1990. Extensions of the Procrustes method for the optimal superimposition of landmarks. Syst. Biol. 39, 40–59.

Rosas, A., Bastir, M., Martínez-Maza, C., García-Tabernero, A., Lalueza-Fox, C., 2006. Inquiries into Neanderthal craniofacial development and evolution: "~~Accretion~~accretion" versus "organismic" models. In: Harvati, K., Harrison, T. (Eds.), Neanderthals Revisited: New Approaches and Perspectives. Springer, Dordrecht, pp. 37–70.

Rosenberger, A.J., Delson, E., 1985. The dentition of *Oreopithecus bambolii*: ~~Systematic~~ systematic and paleobiological implications. Am. J. Phys. Anthropol. 66, 222–223.

Rougier, H., Crevecoeur, I., Beauval, C., Posth, C., Flas, D., Wißing, C., Furtwängler, A., Germonpré, M., Gómez-Olivencia, A., Semal, P., van der Plicht, J., Bocherens, H., Krause, J., 2016. Neandertal cannibalism and Neandertal bones used as tools in ~~Northern~~ northern Europe. Scientific Reports 6, 29005.

Sakai, T., Hanamura, H., 1971. A morphology study of enamel-dentin border on the Japanese dentition. Part V. Maxillary molar. J. Anthropol. Soc. Nippon 79, 297–322.

Salazar-Ciudad, I., Jernvall, J., 2002. A gene network model accounting for development and evolution of mammalian teeth. Proc. Natl. Acad. Sci. 99, 8116–8120.

Salazar-Ciudad, I., Jernvall, J., 2010. A computational model of teeth and the developmental origins of morphological variation. Nature 464, 583–586.

Schüler, T., 2003. ESR dating of a new paleolithic find layer of the travertine site of Weimar-Ehringsdorf (Central Germany). Terra Nostra 2, 233–235.

Schvoerer, M., Rouannet, J.F., Navailles, H., Debenath, A., 1979. Datation absolue par thermoluminescence de restes humains antéwürmiens de l'Abri Suard, à la Chaise de Vouthon (Charente). C. R. Acad. Se. Paris, sér. D. 284, 1979–1982.

Schwarcz, H.P., Debénath, A., 1979. Datation absolue des restes humains de la Chaise-de-Vouthon (Charente) au moyen du déséquilibre des séries d'uranium. C. R. Acad. Se. Paris, sér. D. 288, 1155–1157.

Scott G.R., Turner II, C.G., 1997. The Anthropology of Recent Modern Human Teeth. Dental Morphology and its Variation in Recent Human Populations. Cambridge University Press, Cambridge.

Skelton, R.R., McHenry, H.M., 1986. Phylogenetic analysis of ~~aarlier~~ earlier hominids. Curr. Anthropol. 27, 21–43.

Skinner, M.M., 2008. Enamel-dentine junction morphology of extant hominoid and fossil hominin mandibular molars. Ph.D. Dissertation, The George Washington University.

Skinner, M.M., Gunz, P., 2010. The presence of accessory cusps in chimpanzee mandibular molars is consistent with a patterning cascade model of development. J. Anat. 217, 245–253.

Skinner, M.M., Gunz, P., Wood, B.A., Hublin, J.-J., 2008a. Enamel-dentine junction (EDJ) morphology distinguishes the mandibular molars of *Australopithecus africanus* and *Paranthropus robustus*. J. Hum. Evol. 55, 979–988.

Skinner, M.M., Gunz, P., Wood, B.A., Hublin, J.-J., 2008b. How many landmarks? Assessing the classification accuracy of *Pan* mandibular molars using a geometric morphometric analysis of the occlusal basin as seen at the enamel-dentine junction. Front. Oral. Biol. 13, 23–29.

Skinner, M.M., Wood, B.A., Boesch, C., Olejniczak, A.J., Rosas, A., Smith, T.M., Hublin, J.-J., 2008c. Dental trait expression at the enamel-dentine junction of mandibular molars in extant and fossil hominoids. J. Hum. Evol. 54, 173–186.

Skinner, M.M., Gunz, P., Wood, B.A., Hublin, J.-J., 2009a. Discrimination of extant *Pan* species and subspecies using the enamel-dentine junction morphology of mandibular molars. Am. J. Phys. Anthropol. 140, 234–243.

Skinner, M.M., Wood, B.A., Hublin, J.-J., 2009b. Protostylid expression at the enamel-dentine junction and enamel surface of mandibular molars of *Paranthropus robustus* and *Australopithecus africanus*. J. Hum. Evol. 56, 76–85.

Skinner, M.M., Evans, A., Smith, T., Jernvall, J., Tafforeau, P., Kupczik, K., Olejniczak, A.J., Rosas, A., Radovčić, J., Thackeray, J.F., Toussaint, M., Hublin, J.-J., 2010. ~~Brief communication:~~ Contributions of enamel-dentine junction shape and enamel deposition to primate molar crown complexity. Am. J. Phys. Anthropol. 142, 157–163.

Smith, F.H., Allsworth-Jones, P., Boaz, N.T., 1982. Upper Pleistocene hominid evolution in South-Central Europe: ~~A~~ a review of the evidence and analysis of trends. Curr. Anthropol. 23, 667–703.

~~Strauss, R.E., 2010. Discriminating groups of organisms. In: Elewa, A.M.T. (Ed.), Morphometrics for Nonmorphometricians, Lecture Notes in Earth Sciences. Springer-Verlag, Berlin.~~

Stringer, C.B., Humphrey, L.T., Compton, T., 1997. Cladistic analysis of dental traits in recent humans using a fossil outgroup. J. Hum. Evol. 32, 389–402.

Suwa, G., Wood, B.A., White, T.D., 1994. Further analysis of mandibular molar crown and cusp areas in Pliocene and ~~Earlier~~ earlier Pleistocene hominids. Am. J. Phys. Anthropol. 93, 407–426.

Suzuki, H., 1970. The skull of the Amud man. In: Suzuki, H., Takai, F. (Eds.), The Amud Man and His Cave Site. University of Tokyo Press, Tokyo, pp. 21–52.

Tattersall, I., Schwartz, J.H., 1999. Hominids and hybrids: ~~The~~ the place of Neanderthals in human evolution. Proc. Natl. Acad. Sci. 96, 7117–7119.

Teilhol, V., 2001. Contribution àl'étude individuelle des ossements d'enfants de la-Chaise-de-Vouthon (Charente, France): Approche paléodémographique, paléolithnologique, aspect

morphologique et étude métrique. Place phylogénique des enfants de la Chaise. Ph.D. Dissertation, University of Perpignan.

Thesleff, I., 2000. The genetic basis of tooth development and dental defects. Acta~~.~~ Odontol. Scand. 58, 191–194.

Thesleff, I., 2006. The genetic basis of tooth development and dental defects. Am. J. Med. Genet. Part A~~.~~ 140, 2530–2535.

de Torres, T., Ortiz, J., Grün, R., Eggins, S., Valladas, H., Mercier, N., Tisnérat-Laborde, N., Juliá, R., Soler, V., Martínez, E., Sánchez-Moral, S., Cañaveras, J.C., Lario, J., Badal, E., Lalueza-Fox, C., Rosas, A., Santamaría, D., de la Rasilla, M., Fortea, J., 2010. Dating of the hominid (*Homo neanderthalensis*) remains accumulation from El Sidrón Cave (Piloña, Asturias, North Spain): ~~An~~ an example of a multi-methodological approach to the dating of Upper Pleistocene sites. Archaeometry 52, 680–705.

Trinkhaus, E., 1978. Dental remains from the Shanidar adult Neanderthals. J. Hum. Evol. 7, 369-382.

Turner II, C.G., Nichol, C.R., Scott, G.R., 1991. Scoring procedures for key morphological traits of the permanent dentition: the Arizona State University Dental Anthropology System. In: Kelley, M.A., Larsen, C.S. (Eds.), Advances in Dental Anthropology. Wiley-Liss, New York, pp. 13–31.

Turq, A., Jaubert, J.~~, B, M.~~, Laville, D., 2008. Le cas des sépultures néandertaliennes du Sud-Ouest: Et si on les vieillissait? In: Vandermeersch, B., Cleyet-Merle, J.-J., Jaubert, J., Maureille, B., Turq, A. (Eds.), Première Humanité, Gestes Funéraires Des Néandertaliens. Réunion Des Musées Nationaux, Paris. pp. 40–41.

Tyrrell, A., Chamberlain, A., 1998. Non-metric trait evidence for recent modern human affinities and the distinctiveness of Neanderthals. J. Hum. Evol. 34, 549–554.

Uchida, A., 1998. Variation in tooth morphology of *Gorilla gorilla*. J. Hum. Evol. 34, 55–70.

Valladas, H., Valladas, G., 1991. Datation par la thermoluminescence de silex chauffes des grottes de Kebara et de Qafzeh. In: Bar-Yosef, O., Vandermeersch, B. (Eds.), Le Squelette Moustérien de Kébara 2. Centre National de la Recherche Scientifique, Paris, pp. 43–48.

Valladas, H., Geneste, J.M., Joron, J.L., Chadelle, J.P., 1986. Thermoluminescence dating of Le Moustier (Dordogne, France). Nature 322, 452–454.

Valladas, H., Joron, J.L., Valladas, G., Arensburg, B., Bar-Yosef, O., Belfar-Cohen, A., Goldberg, P., Laville, H., Meignen, L., Rak, Y., Tchernov, E., Tillier, A.-M., Vandermeersch, B., 1987. Thermoluminescence dates for the Neanderthal burial site at Kebara in Israel. Nature 330, 159–160.

Valladas, H., Mercier, N., Froget, L., Hovers, E., Joron, J.-L., Kimbel, W.H., Rak, Y., 1999. TL dates for the Neanderthal site of the Amud Cave, Israel. J. Archaeol. Sci. 26, 259–268.

Vandermeersch, B., 1981. Les Hommes Fossiles de Qafzeh (Israel). Centre National de la Recherche Scientifique, Paris.

Vandermeersch, B., Trinkaus, E., 1995. The postcranial remains of the Régourdou 1 Neandertal: The shoulder and arm remains. J. Hum. Evol. 28, 439–476.

Weaver, T.D., Roseman, C.C., Stringer, C.B., 2007. Were Neandertal and recent modern human cranial differences produced by natural selection or genetic drift? J. Hum. Evol. 53, 135–145.

Weidenreich, F., 1937. The dentition of *Sinanthropus pekinensis*: ~~A~~ a comparative odontography of the hominids. Palaeontol. Sinica D-1, 1–180.

Wild, E.M., Paunovic, M., Rabeder, G., Steffan, I., Steier, P., 2001. Age determination of fossil bones from the Vindija Neanderthal site in Croatia. Radiocarbon 43, 1021–1028.

Wollny, G., Peter, K., Ledesma-Carbayo, M.-J., Skinner, M.M., Hublin, J.-J., Hierl, T., 2013. MIA-A free and open source software for gray scale medical image analysis. Source Code Biol. Med. 8, 20.

Wolpoff, M.H., 1979. The Krapina dental remains. Am. J. Phys. Anthropol. 50, 67–114.

Wolpoff, M.H., Smith, F.H., Malez, M., Radovčić, J., Rukavina, D., 1981. Maxillary Pleistocene human remains from Vindija Cave, Croatia, Yugoslavia. Am. J. Phys. Anthropol. 54, 499–545.

Wood, B.A., Abbott, S.A., 1983. Analysis of the dental morphology of Plio-Pleistocene hominids. I. Mandibular molars: ~~Crown~~ crown area measurements and morphological traits. J. Anat. 136, 197–219.

Wood, R.E., Barroso-Ruíz, C., Caparrós, M., Jordá Pardo, J.F., Galván Santos, B., Higham, T.F.G., 2013. Radiocarbon dating casts doubt on the late chronology of the Middle to Upper Palaeolithic transition in southern Iberia. Proc. Natl. Acad. Sci. 110, 2781-2786.

Zanolli, C., 2015. Brief communication: ~~Molar~~ molar crown inner structural organization in Javanese *Homo erectus*. Am. J. Phys. Anthropol. 156, 148–157.

Zanolli, C., Mazurier, A., 2013. Endostructural characterization of the *H. heidelbergensis* dental remains from the early ~~middle~~ Middle ~~pleistocene~~ Pleistocene site of Tighenif, Algeria. C. R. Palevol. 12, 293–304.

Zanolli, C., Bondioli, L., Mancini, L., Mazurier, A., Widianto, H., Macchiarelli, R., 2012. ~~Brief communication: Two~~ Two human fossil deciduous molars from the Sangiran dome (Java, Indonesia): ~~Outer~~ outer and inner morphology. Am. J. Phys. Anthropol. 147, 472–481.

Zanolli, C., Bondioli, L., Coppa, A., Dean, C.M., Bayle, P., Candilio, F., Capuani, S., Dreossi, D., Fiore, I., Frayer, D.W., Libsekal, Y., Mancini, L., Rook, L., Tekle, T.M., Tuniz, C., Macchiarelli, R., 2014. The late Early Pleistocene human dental remains from Uadi Aalad and Mulhuli-Amo (Buia), Eritrean Danakil: ~~Macromorphology~~ macromorphology and microstructure. J. Hum Evol. 74, 96–113.

Zanolli, C., Grine, F.E., Kullmer, O., Schrenk, F., Macchiarelli, R., 2015. The ~~early~~ Early Pleistocene deciduous hominid molar FS-72 from the Sangiran dome of Java, Indonesia: ~~A~~ a taxonomic reappraisal based on its comparative endostructural characterization. Am. J. Phys. Anthropol. 157, 666–674.

FIGURE CAPTIONS

Figure 1 Landmarking protocol for mandibular and maxillary molars. The EDJ_MAIN landmarks (in red) are placed on the tips of the four primary dentine horns (mandibular molars: 1 = protoconid, 2 = metaconid, 3 = entoconid, 4 = hypoconid; maxillary molars: 1 = protocone, 2 = paracone, 3 = metacone, 4 = hypocone). The EDJ_RIDGE landmarks (in orange) are placed along the marginal ridge of the EDJ. The CEJ_RIDGE landmarks (in blue) are placed along the CEJ. The numbers of landmarks placed along each section of the marginal ridge of the EDJ and along the CEJ are in brackets.

Figure 2 Examples of varying degrees of expression of centrally placed dentine horns. Although there is considerable variation in this trait it is scored as either absent (top) or present (bottom four images).

Figure 3 Post-paracone tubercle. (a) Absent, (b) Minor, (c) Intermediate, (d) Marked. The OES is in the top left corner of each panel. Abbreviations: Pr - protocone, Pa - paracone, Me - metacone, Hy - hypocone.

Figure 4 Crista obliqua type. (a) Absent, (b) Between the metacone and the lingual marginal ridge (or Type I), (c) Between the protocone and metacone (or Type II), (d) Between the lingual marginal ridge and the distal marginal ridge (Type III), (e) Between the protocone and the distal marginal ridge (Type IV), (f) Between the lingual marginal ridge and the metacone and the distal marginal ridge (Type V), (g) Between the protocone and the metacone and the distal marginal ridge (Type VI). The OES is in the top left corner of each panel. Abbreviations: Pr - protocone, Pa - paracone, Me - metacone, Hy - hypocone.

Figure 5 PCA plots of EDJ/CEJ shape and CEJ shape of the mandibular molars. Abbreviations: ENS - earlier Neanderthal sample, LNS - later Neanderthal sample, Hs - recent modern human sample.

Figure 6 Between taxa comparisons of mean EDJ shape of mandibular molars. Abbreviations: Prd - protoconid, Med - metaconid, End - entoconid, Hyd - hypoconulid, Hyp - hypoconid, Pr - protocone, Pa - paracone, Me - metacone, Hy - hypocone.

Figure 7 PCA plots of EDJ/CEJ shape and CEJ shape of the maxillary molars. ENS indicates the earlier Neanderthal sample, LNS indicates the later Neanderthal sample, and Hs indicates the recent modern human sample. Krapina D176 is an earlier Neanderthal sample member M^2 with a reduced hypocone, and therefore groups more closely with the recent modern humans. It is excluded from the convex hull of the earlier Neanderthal sample to show that Neanderthals largely group on one end of PC1, while recent modern humans group on the other side.

Figure 8 Between taxa comparison of mean EDJ shape of maxillary molars. Abbreviations: Prd - protoconid, Med - metaconid, End - entoconid, Hyd - hypoconulid, Hyp - hypoconid, Pr - protocone, Pa - paracone, Me - metacone, Hy - hypocone.

Figure 9 Metameric variation of mean EDJ shape of Neanderthals and recent modern human mandibular and maxillary incisors**.** Abbreviations: Prd - protoconid, Med - metaconid, End - entoconid, Hyd - hypoconulid, Hyp - hypoconid, Pr - protocone, Pa - paracone, Me - metacone, Hy - hypocone.

Figure 10 Boxplot of the natural logarithm of centroid size by molar type. Three stars indicate $p \leq 0.001$, two stars indicate $p \leq 0.01$, one star indicates $p \leq 0.05$, and N.S. indicates $p > 0.05$.

Figure 11 Frequency of centrally placed dentine horns on the mandibular and maxillary molars.

Figure 12 Variation in distal cusp patterning on the maxillary molars (a-f), and the presence of an accessory cusp between the hypoconid and hypoconulid on the mandibular molars (g and h). The OES is in the top left corner of each panel. Abbreviations: Prd - protoconid, Med - metaconid, End - entoconid, Hyd - hypoconulid, Hyp - hypoconid, Pr - protocone, Pa - paracone, Me - metacone, Hy - hypocone.

Figure 13 Examples of twinned dentine horns. The OES is in the top left corner of each panel. Abbreviations: Prd - protoconid, Med - metaconid, End - entoconid, Hyd - hypoconulid, Hyp - hypoconid, Pr - protocone, Pa - paracone, Me - metacone, Hy - hypocone.

TABLES AND FIGURES

Table 1. Study composition and chronological data

Taxa	Chronological attribution	Source for chronology	Locality	EDJ/CEJ sample size	CEJ sample size
Earlier Neanderthal sample	MIS 7	Blackwell and Schwarcz, 1986; Schüler, 2003	Ehringsdorf, Germany	1	6
	MIS 6	Teilhol, 2001	Abri Suard, France	6	6
	MIS 5e	Schvoerer et al., 1979; Schwarcz and Debenath, 1979; Blackwell et al., 1983; Condemi, 2001	Abri Bourgeois-Delaunay, France	3	6
		Rink et al., 1995	Krapina, Croatia	54	69
Later Neanderthal sample	MIS 5c	Ellwood et al., 2004; Pirson et al., 2014	Scladina, Belgium	6	6
	MIS 5c-4	Vandermeersch and Trinkaus, 1995; Delpech, 1996; Turq et al., 2008; Cavanhié, 2010; Bruno Maureille, personal communication	Regourdou, France	2	3
	MIS 5a-4	Guadelli and Laville, 1990	Combe-Grenal, France	5	5
	MIS 4	Valladas et al., 1987; Valladas and Valladas, 1991	Kebara, Israel	0	3
		Guérin et al., 2012	Roc de Marsal, France	2	2
	MIS 4-3	Mercier, 1992; Mercier and Valladas, 1998; Martin, 1920	La Quina France	4	5
	MIS 3	Delson et al., 2000; Valladas et al., 1999; Suzuki, 1970	Amud Cave, Israel	0	3
		Rosas et al., 2006; de Torres et al., 2010	El Sidrón, Spain	13	16
		Valladas et al., 1986; Mellars and Grün, 1991	Le Moustier, France	5	6
		Mercier et al., 1991; Hublin et al., 2012	Saint Césaire, France	3	6
		Wild et al., 2001	Vindija Cave, Croatia	2	8
Recent modern human[1]	MIS 1		Archaeological sites in Belgium	15	15
			Anatomical collections	36	36
			Clinical extractions	55	55

MIS stands for Marine Isotopic Stage. 1. Details about the sample are in SOM Table S1.

Table 2. Neanderthal molars reclassified based on GM analysis of EDJ shape

Specimen	Old identification	Reference	New identification
Combe Grenal IX	M^2	Garralda and Vandermeersch, 2000	M^1
Krapina D101	M^1	Radovčić et al., 1988	M^2
Krapina D104	M_2	Radovčić et al., 1988	M_3
Krapina D105	M_1	Wolpoff, 1979	M_2
Krapina D109	M^3	Wolpoff, 1979	M^2
Krapina D80	M_1	Wolpoff, 1979	M_2
Krapina D9	M_3	Wolpoff, 1979	M_2

Table 3. Classification accuracy of Neanderthal and recent modern human mandibular molars

Molar	Landmarks	Shape/Form	Neanderthal	Human	PCs for CVA
M_1	CEJ	Shape	93.8% (30/32)	95.7% (22/23)	5-19
	EDJ/CEJ	Shape	100% (17/17)	100% (23/23)	5-21
	CEJ	Form	100% (32/32)	91.3% (21/23)	5-12
	EDJ/CEJ	Form	100% (17/17)	100% (23/23)	5-16
M_2	CEJ	Shape	100% (19/19)	95.7% (22/23)	5-16
	EDJ/CEJ	Shape	100% (20/20)	100% (23/23)	5-19
	CEJ	Form	100% (19/19)	100% (23/23)	5-10
	EDJ/CEJ	Form	100% (20/20)	95.7% (22/23)	5-14
M_3	CEJ	Shape	100% (27/27)	100% (17/17)	5-14
	EDJ/CEJ	Shape	93.3% (14/15)	100% (17/17)	5-17
	CEJ	Form	**77.8% (21/27)**	88.2% (15/17)	5-10
	EDJ/CEJ	Form	93.3% (14/15)	100% (17/17)	5-14

Note: Classification accuracies <80% are in bold. The number of PCs used for each CVA is determined as the number of PCs that explain at least 95% of the total variation.

Table 4. Classification accuracy of the earlier and later Neanderthal mandibular molars~~sample, the later Neanderthal sample, and the recent modern human mandibular molars~~

Molar	Landmarks	Shape/Form	Earlier Neanderthal	Later Neanderthal	PCs for CVA
M_1	CEJ	Shape	87.5% (14/16)	81.2% (13/16)	5-15
	EDJ/CEJ	Shape	100% (10/10)	100% (7/7)	5-12
	CEJ	Form	81.2% (13/16)	81.2% (13/16)	5-11
	EDJ/CEJ	Form	80.0% (8/10)	100% (7/7)	5-11
M_2	CEJ	Shape	84.2% (16/19)	83.3% (10/12)	5-13
	EDJ/CEJ	Shape	100% (13/13)	100% (7/7)	5-13
	CEJ	Form	**78.9% (15/19)**	**50.0% (6/12)**	5-10
	EDJ/CEJ	Form	100% (13/13)	100% (7/7)	5-10
M_3	CEJ	Shape	100% (15/15)	91.7% (11/12)	5-11
	EDJ/CEJ	Shape	**71.4% (5/7)**	100% (8/8)	5-10
	CEJ	Form	93.3% (14/15)	83.3% (10/12)	5-7
	EDJ/CEJ	Form	85.7% (6/7)	100% (8/8)	5-9

Note: Classification accuracies <80% are in bold. The number of PCs used for each CVA is determined as the number of PCs that explain at least 95% of the total variation.

Table 5. Classification accuracy of Neanderthal and recent modern human maxillary molars

Molar	Landmarks	Shape/Form	Neanderthal	Human	PCs for CVA
M^1	CEJ	Shape	100% (22/22)	100% (12/12)	5-11
	EDJ/CEJ	Shape	100% (19/19)	100% (12/12)	5-16
	CEJ	Form	100% (22/22)	100% (12/12)	5-7
	EDJ/CEJ	Form	100% (19/19)	100% (12/12)	5-11
M^2	CEJ	Shape	80.0% (20/25)	83.3% (20/24)	5-14
	EDJ/CEJ	Shape	100% (23/23)	100% (24/24)	5-18
	CEJ	Form	92.0% (23/25)	87.5% (21/24)	5-9
	EDJ/CEJ	Form	100% (23/23)	100% (24/24)	5-14
M^3	CEJ	Shape	92.3% (12/13)	100% (7/7)	5-9
	EDJ/CEJ	Shape	100% (12/12)	100% (7/7)	5-12
	CEJ	Form	100% (13/13)	100% (7/7)	5-7
	EDJ/CEJ	Form	100% (12/12)	100% (7/7)	5-10

Note: ~~Classification accuracies <80% are in bold.~~ The number of PCs used for each CVA is determined as the number of PCs that explain at least 95% of the total variation.

Table 6. Classification accuracy of the earlier and later Neanderthal maxillary molar samples

Molar	Landmarks	Shape/Form	Earlier Neanderthal	Later Neanderthal	PCs for CVA
M^1	CEJ	Shape	100% (13/13)	100% (9/9)	5-11
	EDJ/CEJ	Shape	100% (12/12)	100% (7/7)	5-12
	CEJ	Form	100% (13/13)	100% (9/9)	5-8
	EDJ/CEJ	Form	100% (12/12)	100% (7/7)	5-9
M^2	CEJ	Shape	100% (17/17)	100% (8/8)	5-10
	EDJ/CEJ	Shape	100% (16/16)	100% (7/7)	5-12
	CEJ	Form	88.2% (15/17)	**62.5% (5/8)**	5-8
	EDJ/CEJ	Form	100% (16/16)	85.7% (6/7)	5-12
M^3	CEJ	Shape	85.7% (6/7)	83.3% (5/6)	5-8
	EDJ/CEJ	Shape	100% (6/6)	83.3% (5/6)	5-8
	CEJ	Form	85.7% (6/7)	100% (6/6)	5-6
	EDJ/CEJ	Form	100% (6/6)	83.3% (5/6)	5-8

Note: Classification accuracies <80% are in bold. The number of PCs used for each CVA is determined as the number of PCs that explain at least 95% of the total variation.

Table 7. Between group pairwise comparisons of molar size (centroid size)

Comparison	M_1	M_2	M_3	M^1	M^2	M^3
Neanderthal vs. modern human	**0.001**	**< 0.001**	**0.002**	**0.001**	**< 0.001**	**0.031**
Earlier vs. later Neanderthal	0.900	0.797	0.327	0.215	0.414	0.711
Earlier Neanderthal vs. modern human	**0.005**	**< 0.001**	0.075	**< 0.001**	**< 0.001**	0.099
Later Neanderthal vs. modern human	**0.009**	**0.001**	**0.002**	0.069	**< 0.001**	**0.042**

Note: *p*-values were calculated using a Kruskal-Wallis one-way analysis of variance test

Table 8. Within group pairwise comparisons of molar[1] size (centroid size)

		M1	M2	M3
Neanderthals	M1		0.158	**< 0.001**
	M2	0.919		**0.003**
	M3	**0.028**	**0.017**	
		M1	M2	M3
Recent modern humans	M1		**0.024**	**0.006**
	M2	0.139		0.246
	M3	**0.018**	0.322	
		M1	M2	M3
Earlier Neanderthal	M1		0.106	**< 0.001**
	M2	0.809		**0.011**
	M3	**0.039**	**0.017**	
		M1	M2	M3
Later Neanderthal	M1		0.778	0.065
	M2	0.879		0.115
	M3	0.244	0.316	

Note: 1. *p*-values for maxillary molar comparisons in maxillary right quadrant and mandibular molar comparisons in mandibular left quadrant. *p*-values were calculated using a Kruskal-Wallis one-way analysis of variance test.

Formatted: Font: Italic

Formatted: Font: Italic

Table 9. Frequency of centrally placed dentine horn tips on mandibular and maxillary molars

Group	Protoconid	Metaconid	Entoconid	Hypoconulid	Hypoconid
Earlier Neanderthal	0/24 (0%)	24/28 (85.7%)	17/24 (70.8%)	0/21 (0%)	0/10 (0%)
Later Neanderthal	3/13 (23.1%)	19/20 (95.0%)	10/16 (62.5%)	1/21 (4.8%)	0/19 (0%)
Recent modern human	1/44 (2.3%)	20/56 (35.7%)	21/60 (35.0%)	2/48 (4.2%)	0/60 (0%)

Group	Protocone	Paracone	Metacone	Hypocone
Earlier Neanderthal	1/27 (3.7%)	6/30 (20.0%)	14/32 (43.8%)	0/32 (0%)
Later Neanderthal	2/17 (11.8%)	5/17 (29.4%)	0/19 (0%)	0/19 (0%)
Recent modern human	0/43 (0%)	11/40 (27.5%)	6/43 (14.0%)	1/43 (2.3%)

Table 10. Frequency of the post-paracone tubercle

Group	Molar	*n*	Absent	Minor	Intermediate	Marked
Earlier Neanderthal	M^1	12		25%	58%	17%
	M^2	16		81%	19%	
	M^3	6		83%	17%	
Later Neanderthal	M^1	7		29%	43%	28%
	M^2	7		86%	14%	
	M^3	6		83%		17%
Recent modern human	M^1	12	8%	92%		
	M^2	24	21%	75%	4%	
	M^3	7		57%	29%	14%

Formatted: Font: Italic

Table 11. Frequency of crista obliqua type

Group	Molar	*n*	Absent	I	II	III	IV	V	VI
Earlier Neanderthal	M^1	12		100%					
	M^2	16	6%	6%	88%				
	M^3	6				83%		17%	
Later Neanderthal	M^1	7		71%	29%				
	M^2	7		14%	72%	14%			
	M^3	6		17%		33%	33%		17%
Recent modern human	M^1	12		92%	8%				
	M^2	24	13%	50%	25%			8%	4%
	M^3	7	43%		14%	29%	14%		

Formatted: Font: Italic

Figure1

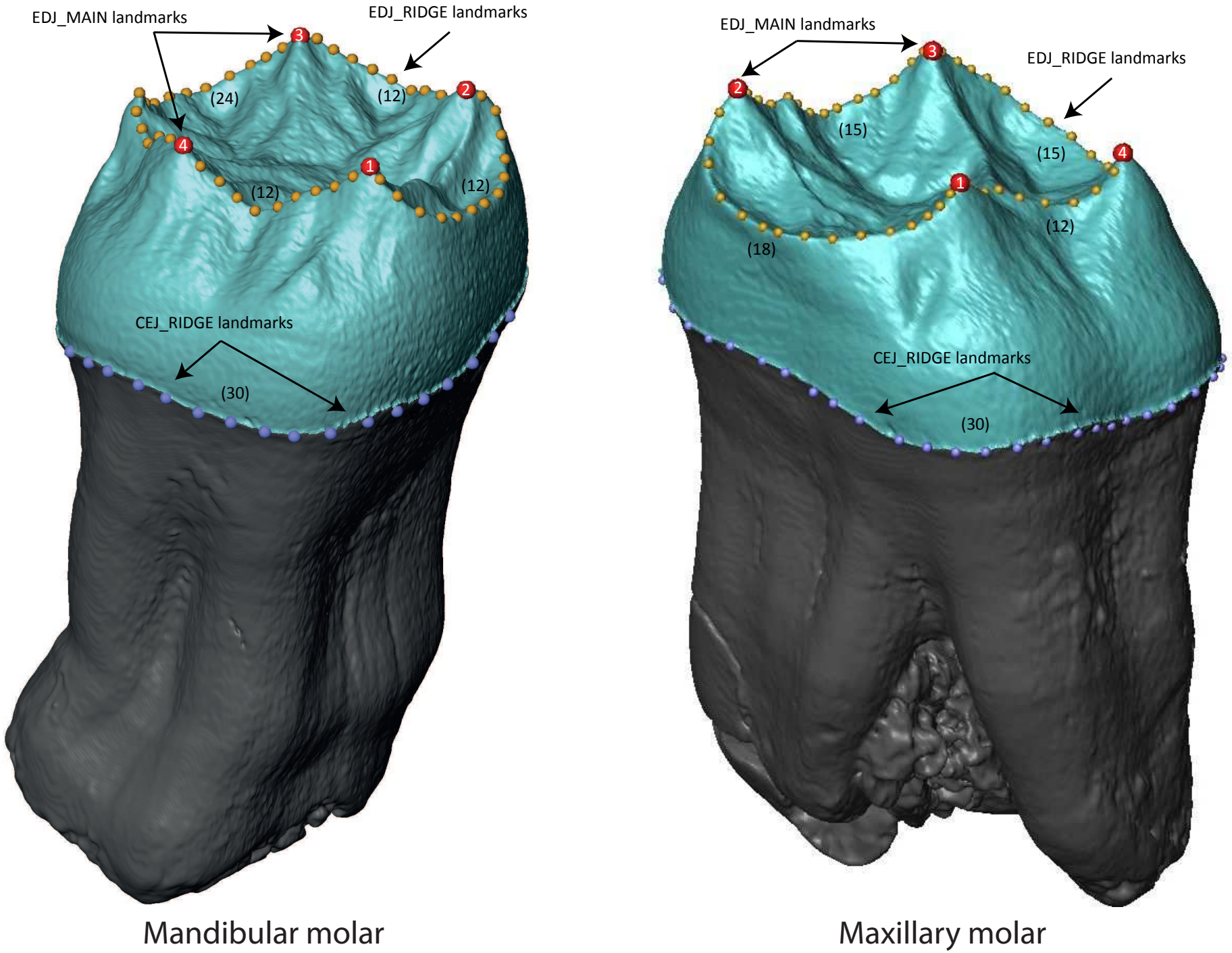
EDJ_MAIN landmarks
EDJ_RIDGE landmarks
3
2
4
1
(24)
(12)
(12)
(12)
CEJ_RIDGE landmarks
(30)
Mandibular molar
EDJ_MAIN landmarks
EDJ_RIDGE landmarks
3
2
4
1
(15)
(15)
(12)
(18)
CEJ_RIDGE landmarks
(30)
Maxillary molar

Figure2

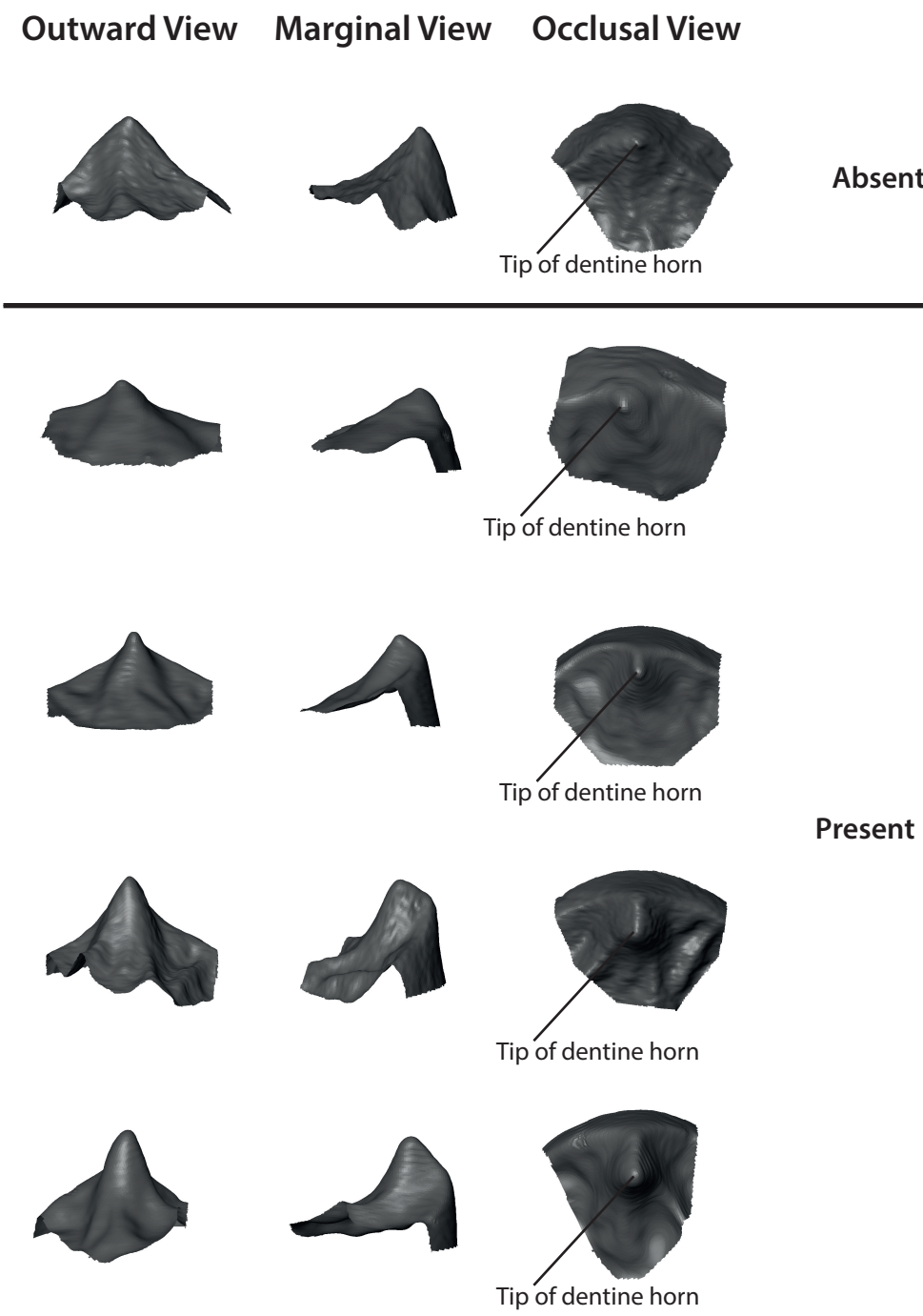
Outward View
Marginal View
Occlusal View
Tip of dentine horn
Absent
Tip of dentine horn
Tip of dentine horn
Present
Tip of dentine horn
Tip of dentine horn

Figure3

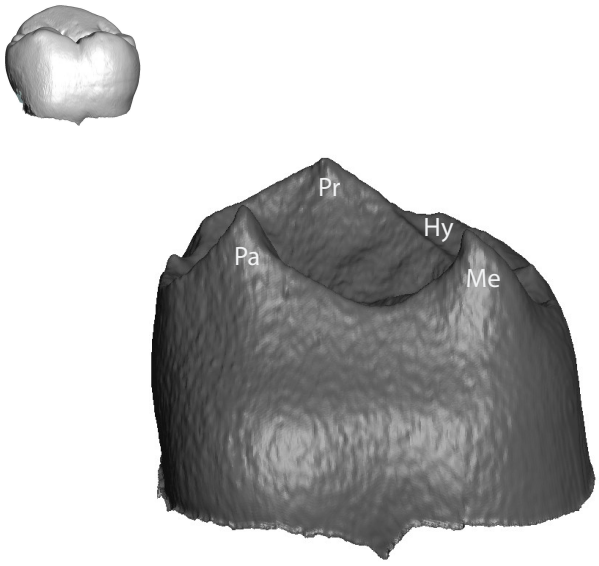

(a) ABSENT - MPI M189 M^2 Left (mirrored)

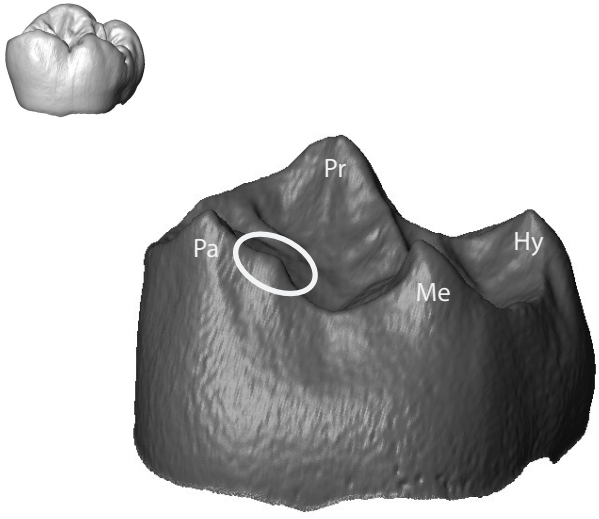

(b) MINOR - Krapina D98 M^2 Right

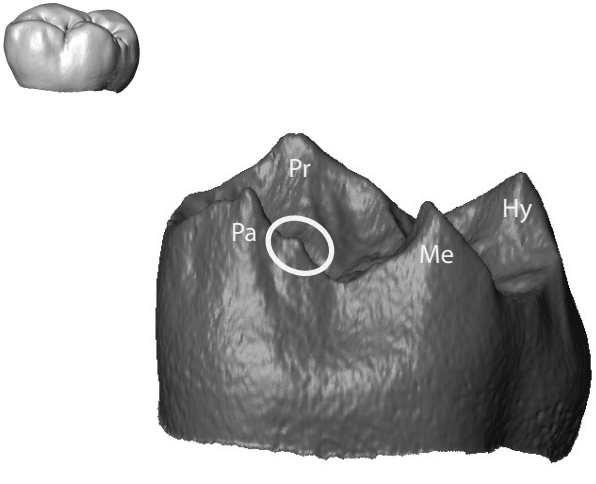

(c) INTERMEDIATE - Krapina D171 M^1 Right

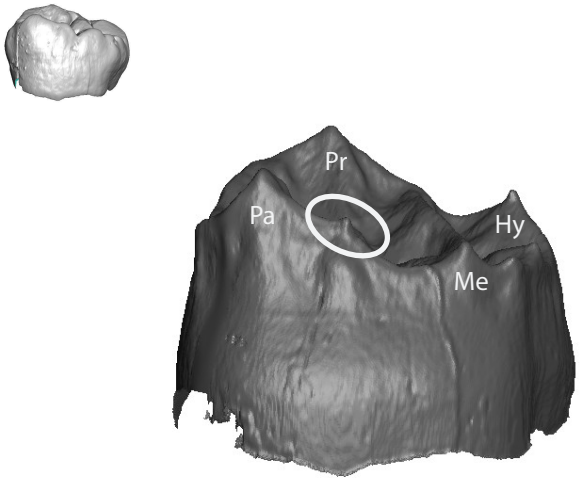

(d) MARKED - El Sidrón SD1164 M^3 Right

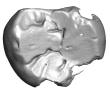

Absent

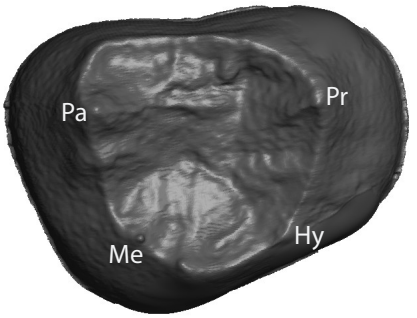

(a) Krapina D176 M^2 Left (mirrored)

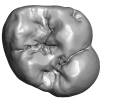

Type I

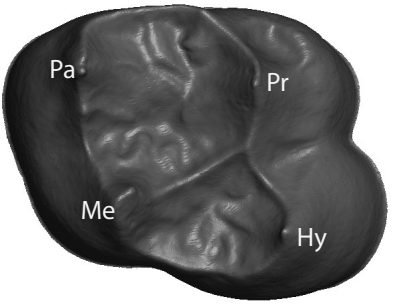

(b) Krapina 45 M^1 Left (mirrored)

Type II

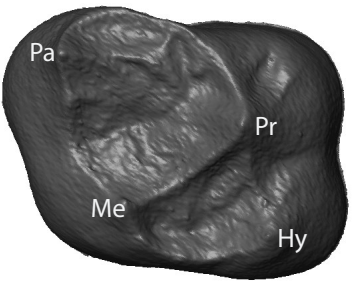

(c) Krapina D169 M^2 Right

Type III

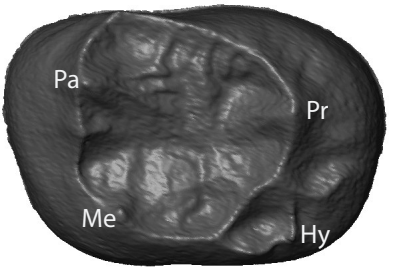

(d) Krapina D163 M^3 Right

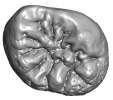

Type IV

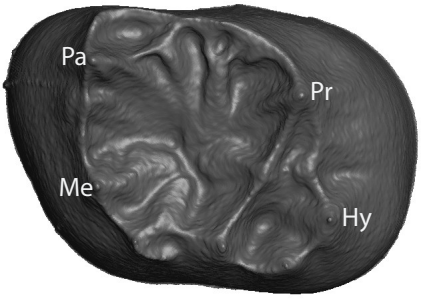

(e) El Sidrón SD621 M^3 Right

Type V

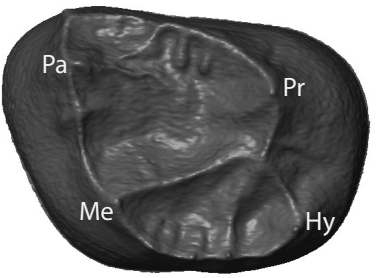

(f) Krapina D170 M^3 Right

Type VI

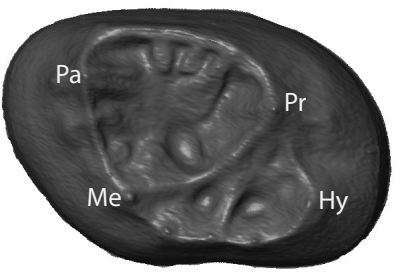

(g) El Sidrón SD332 M^3 Left (mirrored)

Figure5

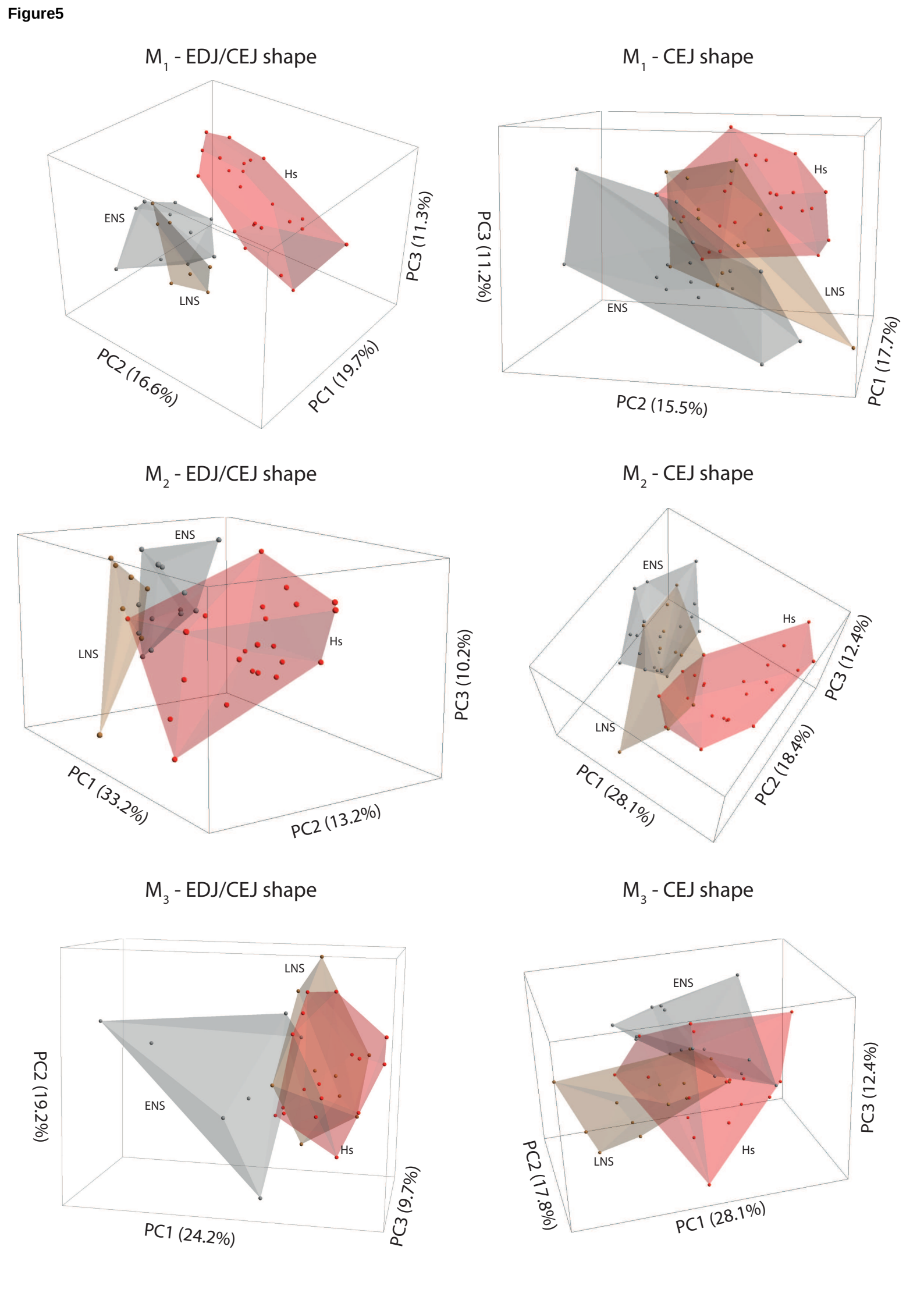
M1 - EDJ/CEJ shape
Hs
ENS
LNS
PC3 (11.3%)
PC2 (16.6%)
PC1 (19.7%)
M1 - CEJ shape
Hs
LNS
ENS
PC3 (11.2%)
PC2 (15.5%)
PC1 (17.7%)
M2 - EDJ/CEJ shape
ENS
LNS
Hs
PC3 (10.2%)
PC1 (33.2%)
PC2 (13.2%)
M2 - CEJ shape
ENS
Hs
LNS
PC3 (12.4%)
PC1 (28.1%)
PC2 (18.4%)
M3 - EDJ/CEJ shape
LNS
ENS
Hs
PC2 (19.2%)
PC1 (24.2%)
PC3 (9.7%)
M3 - CEJ shape
ENS
LNS
Hs
PC2 (17.8%)
PC1 (28.1%)
PC3 (12.4%)

Figure6

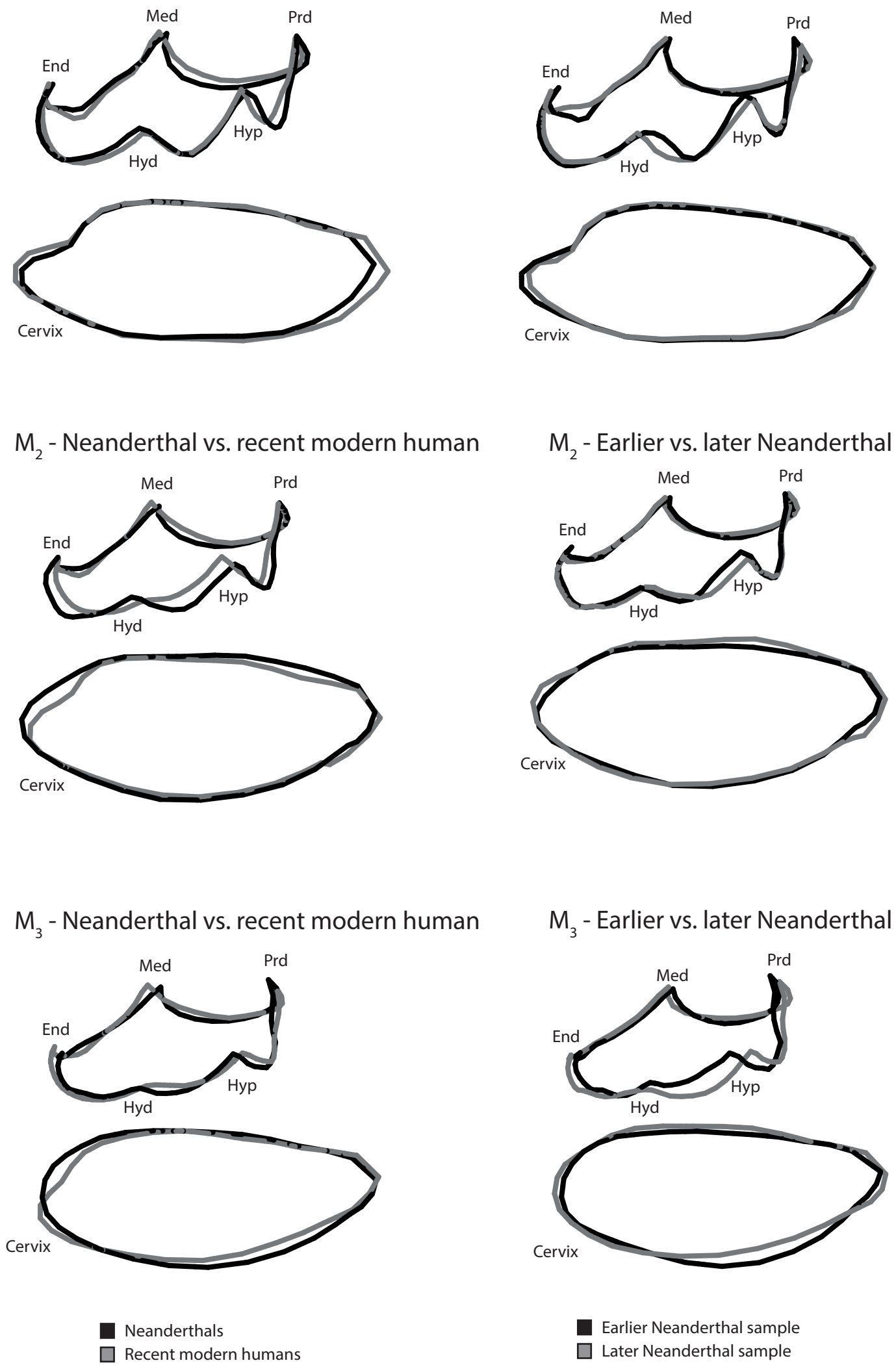
M1 - Neanderthal vs. recent modern human
Med
Prd
End
Hyp
Hyd
Cervix
M1 - Earlier vs. later Neanderthal
Med
Prd
End
Hyp
Hyd
Cervix
M2 - Neanderthal vs. recent modern human
Med
Prd
End
Hyp
Hyd
Cervix
M2 - Earlier vs. later Neanderthal
Med
Prd
End
Hyp
Hyd
Cervix
M3 - Neanderthal vs. recent modern human
Med
Prd
End
Hyp
Hyd
Cervix
M3 - Earlier vs. later Neanderthal
Med
Prd
End
Hyp
Hyd
Cervix
Neanderthals
Recent modern humans
Earlier Neanderthal sample
Later Neanderthal sample

Figure7

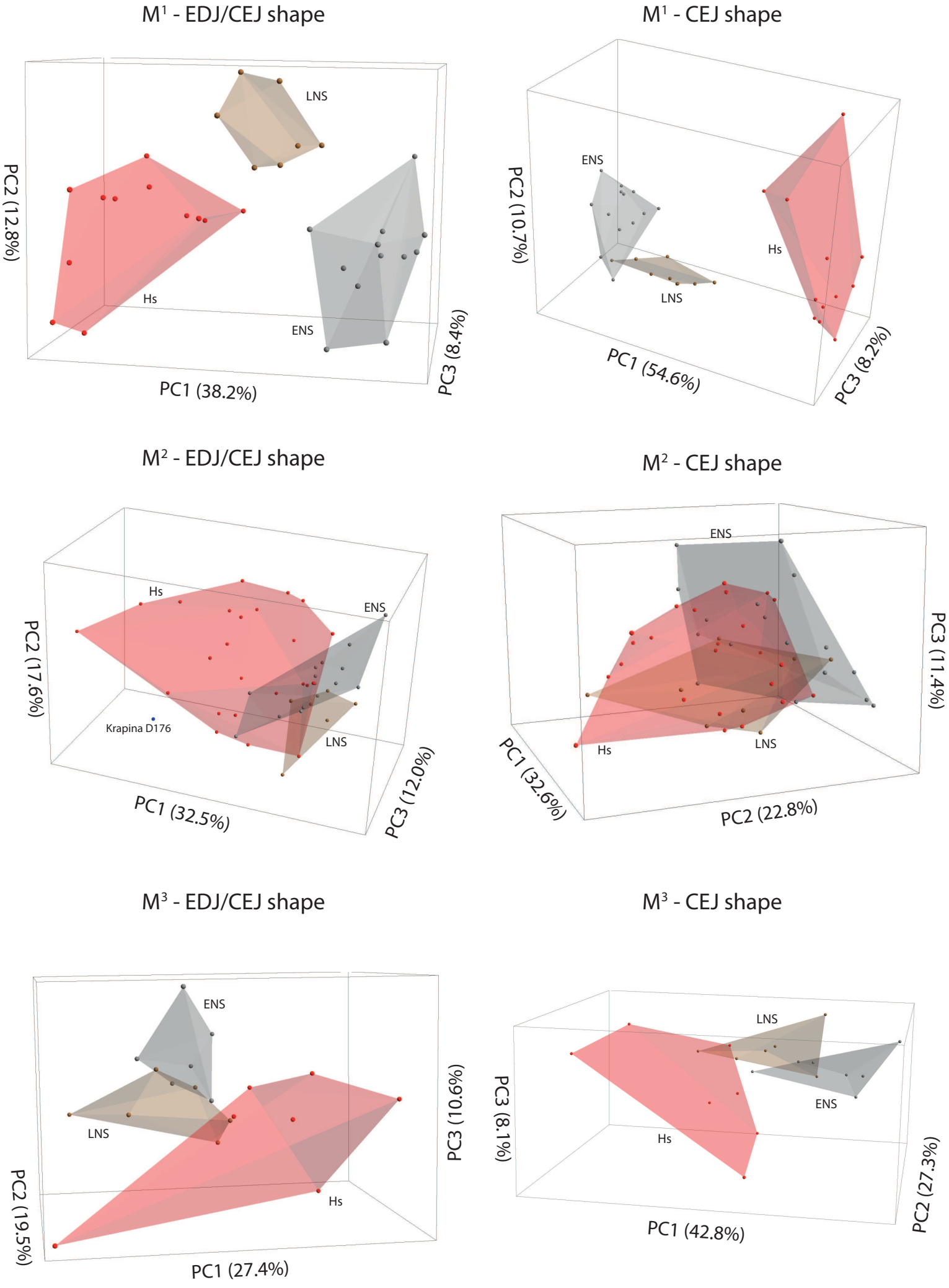
M1 - EDJ/CEJ shape
LNS
Hs
ENS
PC2 (12.8%)
PC1 (38.2%)
PC3 (8.4%)
M1 - CEJ shape
ENS
Hs
LNS
PC2 (10.7%)
PC1 (54.6%)
PC3 (8.2%)
M2 - EDJ/CEJ shape
Hs
ENS
Krapina D176
LNS
PC2 (17.6%)
PC1 (32.5%)
PC3 (12.0%)
M2 - CEJ shape
ENS
Hs
LNS
PC3 (11.4%)
PC1 (32.6%)
PC2 (22.8%)
M3 - EDJ/CEJ shape
ENS
LNS
Hs
PC2 (19.5%)
PC1 (27.4%)
PC3 (10.6%)
M3 - CEJ shape
LNS
ENS
Hs
PC3 (8.1%)
PC1 (42.8%)
PC2 (27.3%)

Figure8

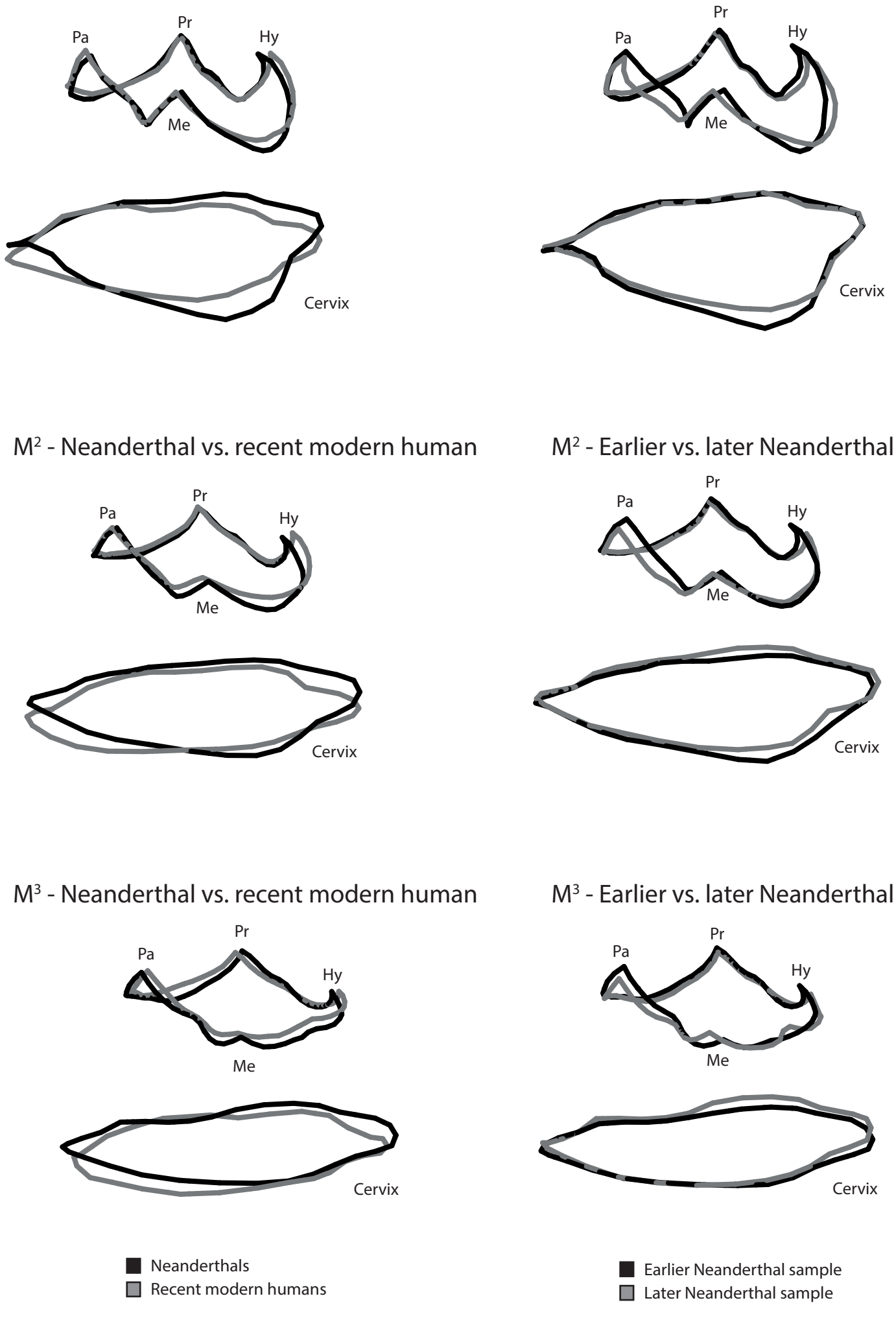
M1 - Neanderthal vs. recent modern human
Pa
Pr
Hy
Me
Cervix
M1 - Earlier vs. later Neanderthal
Pa
Pr
Hy
Me
Cervix
M2 - Neanderthal vs. recent modern human
Pa
Pr
Hy
Me
Cervix
M2 - Earlier vs. later Neanderthal
Pa
Pr
Hy
Me
Cervix
M3 - Neanderthal vs. recent modern human
Pa
Pr
Hy
Me
Cervix
M3 - Earlier vs. later Neanderthal
Pa
Pr
Hy
Me
Cervix
Neanderthals
Recent modern humans
Earlier Neanderthal sample
Later Neanderthal sample

Figure9

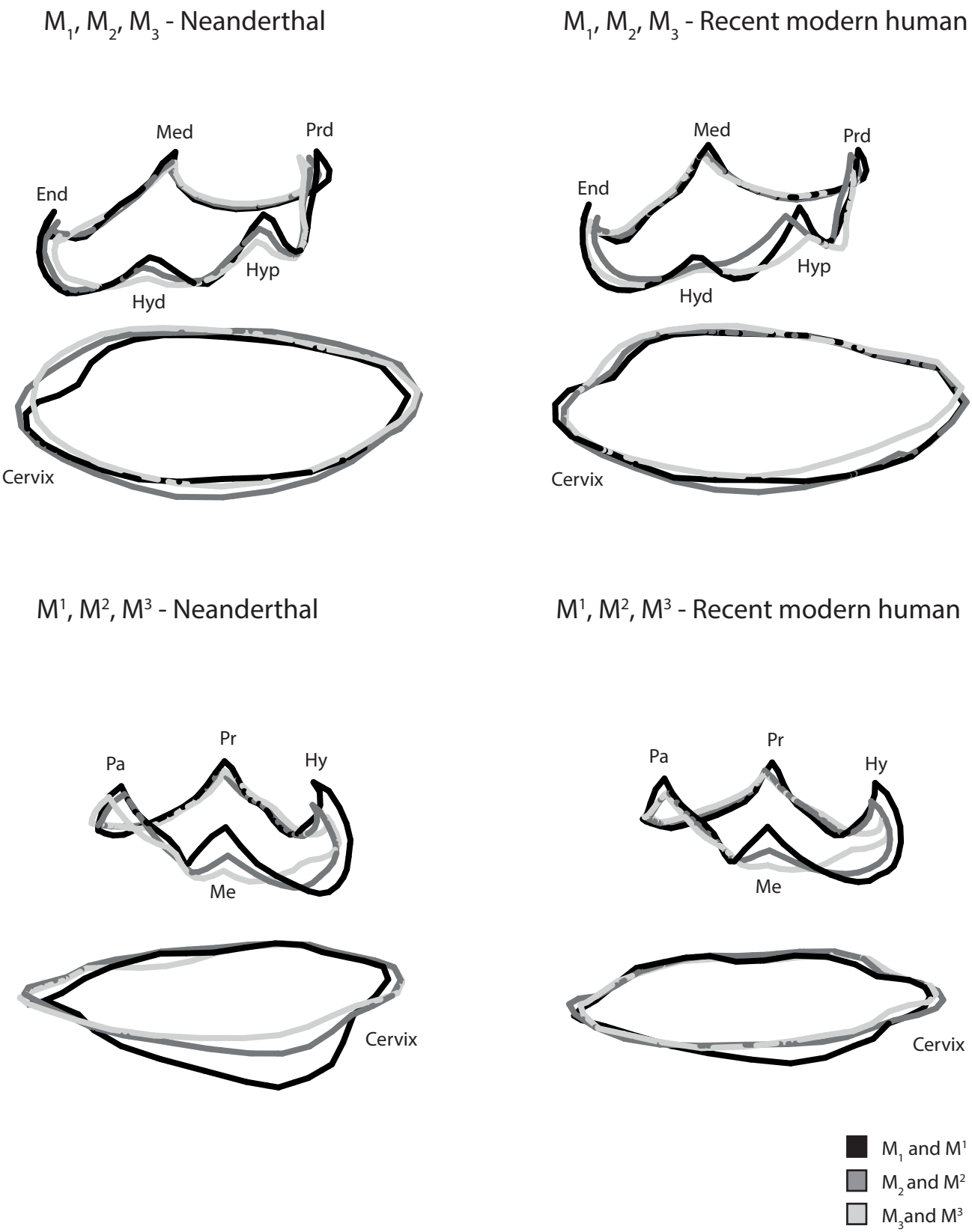
M1, M2, M3 - Neanderthal
Med
Prd
End
Hyp
Hyd
Cervix
M1, M2, M3 - Recent modern human
Med
Prd
End
Hyp
Hyd
Cervix
M1, M2, M3 - Neanderthal
Pr
Pa
Hy
Me
Cervix
M1, M2, M3 - Recent modern human
Pr
Pa
Hy
Me
Cervix
M1 and M1
M2 and M2
M3and M3

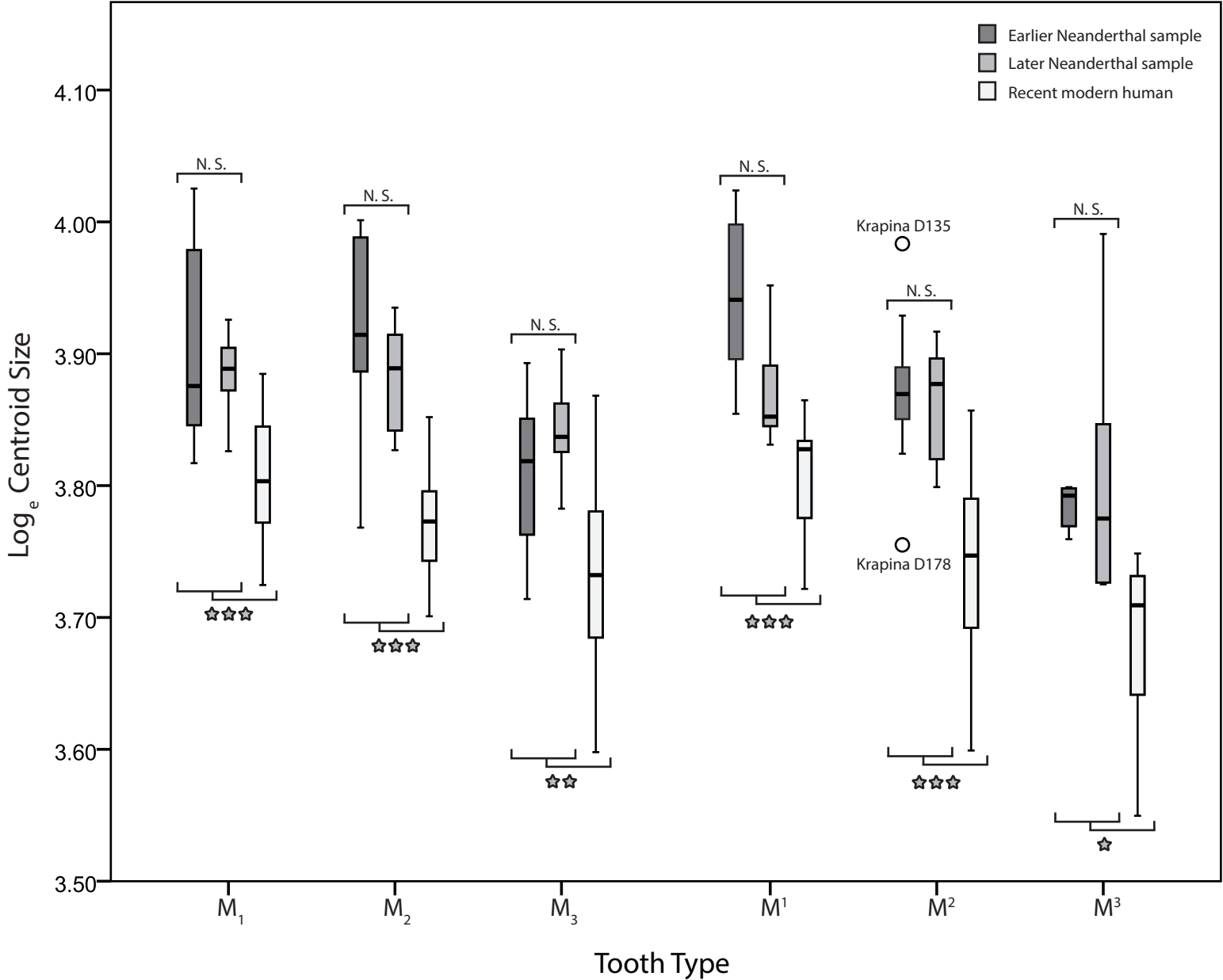
Earlier Neanderthal sample
Later Neanderthal sample
Recent modern human
4.10
4.00
3.90
3.80
3.70
3.60
3.50
Log e Centroid Size
N. S.
N. S.
N. S.
N. S.
Krapina D135
N. S.
Krapina D178
N. S.
M1
M2
M3
M1
M2
M3
Tooth Type

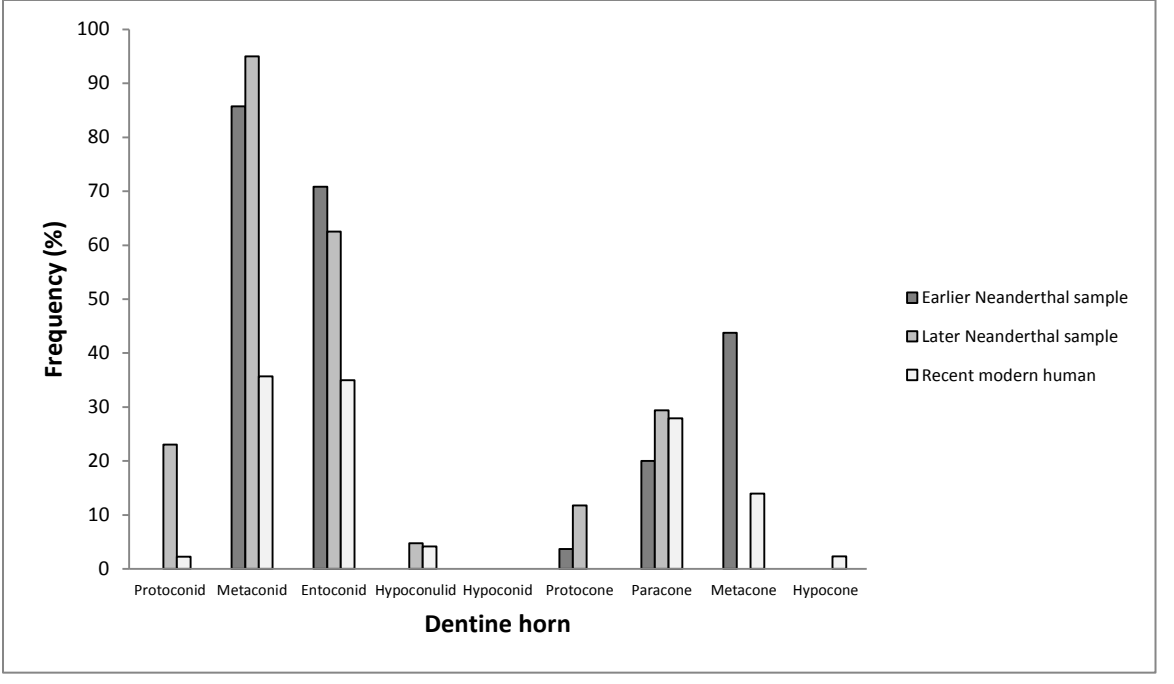
100
90
80
70
60
50
40
30
20
10
0
Frequency (%)
Protoconid
Metaconid
Entoconid
Hypoconulid
Hypoconid
Protocone
Paracone
Metacone
Hypocone
Dentine horn
Earlier Neanderthal sample
Later Neanderthal sample
Recent modern human

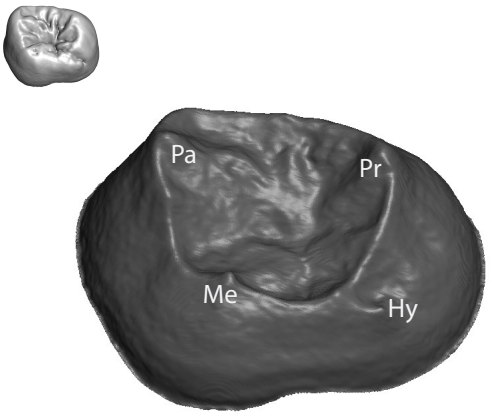

(a) Krapina D97 M^3 Right

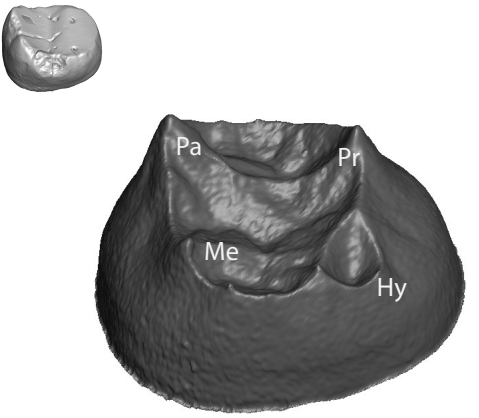

(b) Krapina D173 M^3 Right

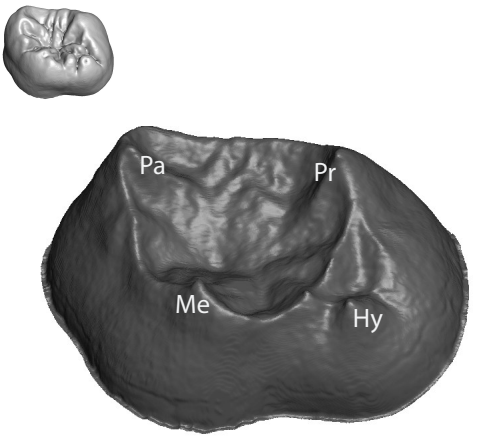

(c) Abri Bourgeois-Delaunay BD8 M^3 Left (mirrored)

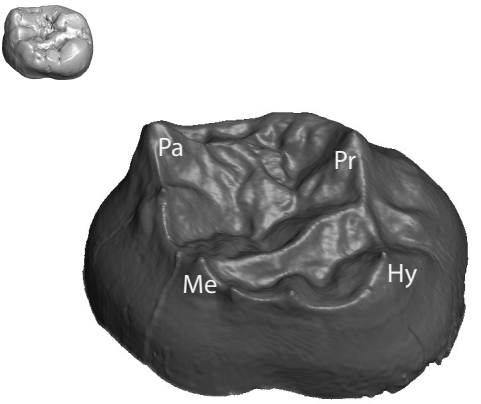

(d) El Sidrón SD1164 M^3 Right

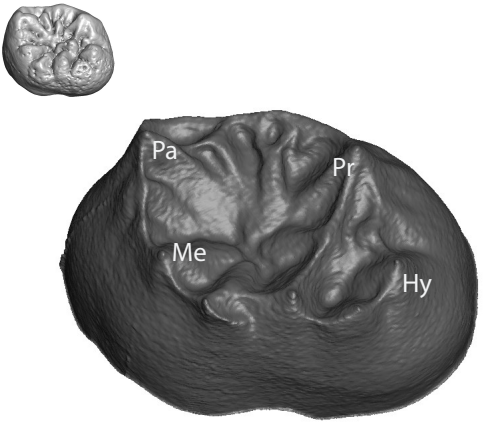

(e) El Sidrón SD621 M^3 Right

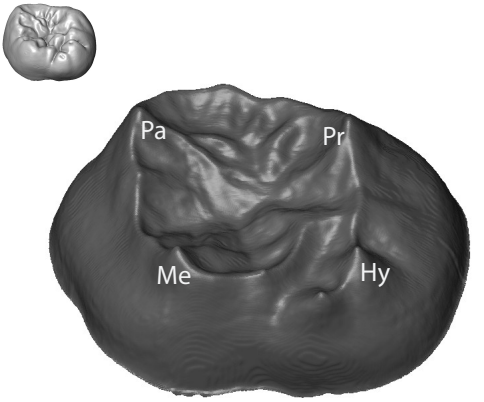

(f) Scladina 4A_3 M^2 Right

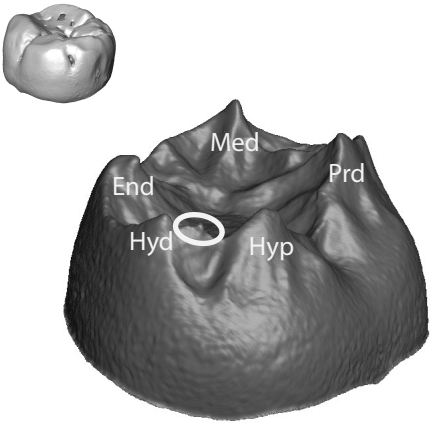

(g) Abri Suard S36 M_2 Left (mirrored)

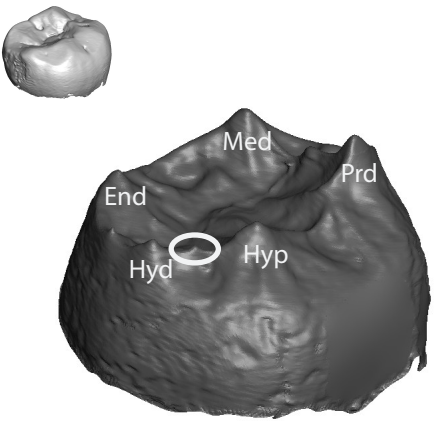

(h) La Quina Q760_H9 M_2 Left (mirrored)

Figure13

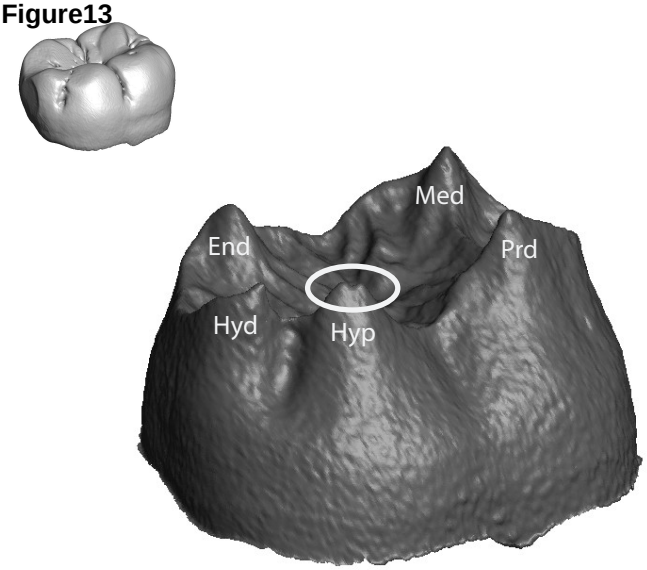

(a) Krapina 54 M_1 Left (mirrored)

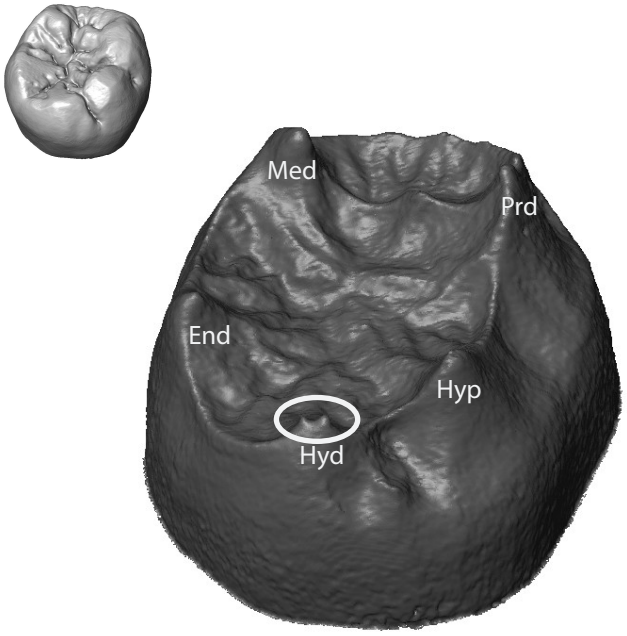

(b) Combe-Grenal I M_1 Right

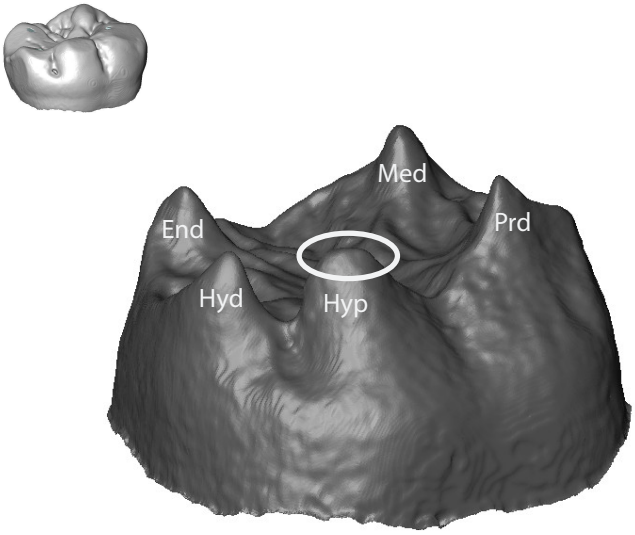

(c) Krapina D79 M_1 Right

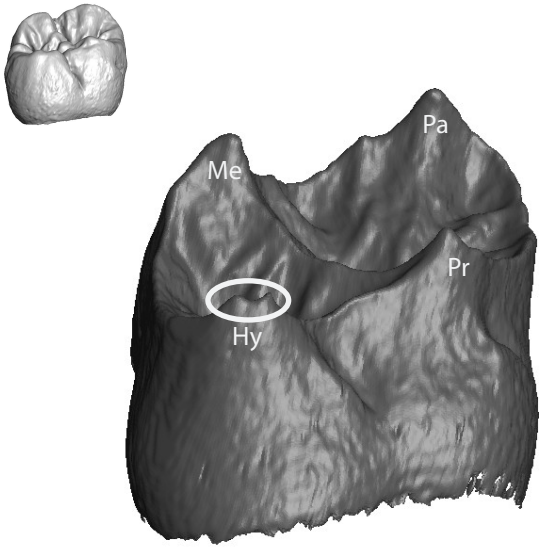

(d) Roc de Marsal M^1 Left (mirrored)

Supplementary Material

Click here to download Supplementary Material: Martin et al_SI_v2_CH_MS.docx